Resonant Cavity Antenna Arrays: Performance Investigation and Characterization

By

Arslan Kiyani

A thesis submitted to Macquarie University

for the degree of Master of Research

Department of Engineering

April 2016

MACQUARIE
University
SYDNEY·AUSTRALIA

Typeset in LaTeX 2_ε.

The work presented in this thesis was carried out at the Department of Engineering, Macquarie University, Sydney, Australia, between July 2015 and April 2016. This work was principally supervised by Professor Karu Esselle and the co-supervision was done by Dr. Raheel Maqsood Hashmi. Except where acknowledged in the customary manner, the material presented in this thesis is, to the best of my knowledge, original and has not been submitted in whole or part for a degree in any other university or institution other than Macquarie University.

Arslan Kiyani

Acknowledgments

I would like to express my deepest and sincerest gratitude to my principal supervisor, Professor Karu P. Esselle, for his excellent support and quality supervision during this research work. I highly acknowledge his invaluable guidance and encouragement for successful and timely completion of this milestone.

I am highly indebted to my co-supervisor, Dr. Raheel M. Hashmi, for his guidance and constant support throughout this research. I offer special thanks to you for your thorough monitoring and valuable feedback that uplifted the quality of this work.

I would also like to acknowledge Macquarie University for awarding me the international Research Training Pathway Scholarship (iRTP).

I will always be grateful for the support and encouragement that I received from my fellow researchers of Group "Centre for Collaboration in Electromagnetic and Antenna Engineering". I am thankful to all of them for providing a healthy and friendly work environment. Especially, I cannot forget the help and encouragement I got from Dr. Muzahir Abbas, Mr. Usman Afzal, Mr. Ali Lalbakhsh and Mr. Affaz aziz.

I would like to offer my fondest regards to my family. I am incredibly grateful to my parents who always supported me and remained a constant source of prayers and motivation. Last but not the least, I would like to thank all my friends for their good wishes, hospitality, and encouragement from time to time.

List of Publications

- **Arslan Kiyani**, Raheel M. Hashmi and Karu P. Esselle, *"Planar Feeding Technique for Wideband, Low-Profile Resonant Cavity Antennas*," IEEE International Symposium on Antennas and Propagation (APS), Puerto Rico, 2016.

- **Arslan Kiyani**, Raheel M. Hashmi and Karu P. Esselle, *"Performance Evaluation of Conventional and Planar Feeds in Resonant Cavity Antennas*," Advanced Electromagnetics Symposium, Malaga, Spain 2016.

Abstract

This thesis investigates the feasibility of developing wideband resonant cavity antennas (RCAs) to achieve ETSI Class-2 antenna requirements for operation in 21.2-23.6 GHz frequency band. Commercially available Class-2 reflector antennas have strict requirements to conform to the suitable radiation pattern envelope (RPE) specifications, as set by the regulatory bodies. Despite excellent performance of commercial Class-2 compliant antennas, a major geometrical constraint prevails due to their non-planar, complex, multi-piece and bulky structures. RCAs on the other hand, are well known for their simple and planar configurations. With rapid advancements in modern wireless technologies, RCAs have found numerous applications from indoor personal communications to wireless sensor networks, and from point-to-point communications to satellite reception. This thesis investigates the possibility of developing wideband and high-gain resonant cavity antenna arrays (RCAAs), to combine the advantages of low-cost, planar configuration with high efficiency and compactness.

Contents

List of Figures

List of Tables

Chapter 1

Introduction

1.1 Background

Wireless communication systems have seen tremendous growth in recent years. Cutting-edge wireless technologies have revolutionized the communication world with ever-increasing data rates and improved reliability. Considering recent advancements, there is a constant need to design and investigate new components to support and improve these technologies. Antennas act as a vital front end component of any wireless system. Modern wireless systems require high performance, cost-effective antennas to cope up with the competitive demands of increased coverage, higher data rates and reduced interference. Interference is a very critical parameter in modern antenna systems and is often controlled by forcing antenna to comply with standardized radiation pattern envelopes (RPEs)[1]. Recently, the use of planar, high gain antennas in numerous applications such as backhaul systems, wireless sensor networks, short-range to medium-range directional communications and satellite reception has seen increased interest. Conventional parabolic reflectors and phased arrays have always been the capstone in the domain of high gain antennas. However, despite their excellent performance, the bulky nature of parabolic reflectors makes them physically unattractive for various applications. On the other hand, phased arrays are constrained by high design complexity and expensive amplifier modules to combat power losses. Recently, resonant cavity antenna (RCA) has emerged as a potential alternative for high gain applications.

Table 1.1: Specifications of the back-haul antennas for fixed wireless communication applications, particularly point-to-point communications (as documented by ETSI)

Frequency Band	21.2 - 23.6 GHz
% Bandwidth	10.7
Gain	37 dBi
RPEs	Class-2

Table 1.2: ETSI specifications for the Class-2 antennas RPE

Angle (°)	**RPE Value (dBi)**
5	20
10	12
20	10
50	2

1.2 Motivation of the Research

Fixed wireless systems serve as the backbone of high-speed data services in metropolitan areas and urban environments. These systems are targeted to support base station antennas through back-haul networks, and point-to-point microwave links. Fixed wireless communication systems largely deploy reflectors (compliant with Class-2 RPEs) to improve the signal quality and expand the network coverage. However, the commercial Class-2 compliant antennas are required to meet the strict requirements of gain and suitable radiation pattern envelope (RPE) specifications, as set by the regulatory authorities of ETSI[2]. The minimum antenna specifications and corresponding RPEs defined by the ETSI for fixed communication applications are provided in Table 1.1 and Table 1.2 respectively. Although many Class-2 reflectors are available commercially, yet several challenges need to be overcome to address the increasing demands of planar, concealable systems. These challenges include planar configurations, compactness, simple feed mechanisms, light weight and low manufacturing

[1]RPE is a straight line segmented graphical representation of the antenna radiation patterns. RPEs play a significant role in the planing and operation of microwave links and networks.

[2]European Telecommunications Standards Institute

cost. This implies the need to shift the research focus on alternative antenna solutions.

RCA is a class of highly directive antennas having planar structure, simple configuration, and low-profile characteristics. RCAs are being viewed as the emerging candidates for use in modern communication systems. Despite a number of advantages of RCAs, the main factor that limits their utilization in some applications is the narrow bandwidth behavior and gain up to 20 dBi. This gives the motivation to design wideband resonant cavity antenna arrays (RCAAs) and investigate their potential for satisfying the minimum ETSI Class-2 antenna requirements, as specified in Table 1.1 and Table 1.2.

1.3 Research Framework and Objectives

This thesis has been carried out towards Master of Research (MRes) degree at the Center for Collaboration in Electromagnetic and Antenna Engineering in the Department of Engineering, Faculty of Science at Macquarie University, Sydney, Australia. The research was fully funded by an international Research Training Pathway Scholarship (iRTP) award. The project spanned over 9 months, initiating in July 2015. Based on *Macquarie University MRes thesis guidelines*, the main body of this thesis is limited to a maximum of 50 pages, approximately.

The primary objective of this thesis is the performance investigation and characterization of resonant cavity antenna arrays (RCAAs), as a potential alternative for conventional high-gain antennas. To accomplish this, the initial objective is to design a single RCA element. The RCA with transverse permittivity gradient (TPG) based superstrate is considered with smaller footprint area and excellent directive characteristics suitable for array implementation. Hence, the second objective is to develop wideband and highly-directive RCAAs with low side lobe levels (SLLs) and appropriate RPEs. It is imperative to analyze the performance parameters (as given in Table 1.1 and Table 1.2 respectively) to estimate the potential of designed RCAAs. Following this, the third objective is to investigate the possibility of improving far-field radiation characteristics of RCAAs through the implementation of a phase correction technique. Lastly, the final objective is set to evaluate the performance of wideband RCAs by employing planar feeding techniques, which can easily be extended for use in sparse arrays.

1.4 Thesis Organization and Contributions

The thesis consists of seven chapters, including this brief introductory chapter and concluding remarks in Chapter 7. The remaining 5 chapters are organized as follows:

Chapter 2 presents an overview of RCAs along with various analytical methods that have been used for their characterization in the past. A generalized literature progress towards wideband RCAs is also included in this chapter. However, it should be remarked that the related literature review is presented at the beginning of each chapter, accordingly.

In Chapter 3, the design of a low-profile, wideband RCA is presented. The RCA is shown to employ a single-layer dielectric superstrate which has radially non-uniform permittivity in lateral dimensions. This configuration allows RCA to radiate efficiently with 3dB directivity bandwidth and 3dB gain bandwidth complementing each other. Furthermore, excellent wide band matching of more than 20% is achieved with the peak directivity of 18.7 dBi and 3dB directivity bandwidth of 49.31%. This RCA is well suited for the design of RCA arrays.

Chapter 4 utilizes the RCA element proposed in Chapter 3 to investigate and characterize a new class of RCA arrays. Theoretical array characteristics are studied in detail. Two actual array topologies have been employed based on square and radial array configurations using full-wave analysis. Numerical results of a 9×9 square array and Tier7[3] radial array are presented and compared. It is shown that Tier7 radial array has the potential to satisfy minimum ETSI Class-2 antenna requirements with appropriate RPEs and SLLs as low as -17 dBi. These arrays have a significant advantage of planar configuration and compactness.

Chapter 5 presents the design and implementation of an all-dielectric phase correcting surface (PCS), with the aim of improving the radiation characteristics of RCAAs. A thorough discussion entailing the aperture phase distribution maps is presented. The all-dielectric PCS demonstrated a slight improvement of 0.6 dBi in the peak directivity and 1.8 dBi reduction in the SLL at the operating frequency of 22.3 GHz.

Chapter 6 addresses a few limitations associated with conventional waveguide feed by evaluating the planar feeding techniques for use in wideband RCAs. An efficient feeding method based on single/dual aperture coupled slot is demonstrated to obtain peak directivity of 16-17 dBi with a well-matched bandwidth of 20%. The use of planar feed reduces the

[3]Radial array with 7 elements is referred to as Tier1, radial array with 91 elements is referred to as Tier7.

overall height of the RCA as compared to a waveguide feed. The results of this work are presented in the following publications.

- **Arslan Kiyani**, Raheel M. Hashmi and Karu P. Esselle, *"Planar Feeding Technique for Wideband, Low-Profile Resonant Cavity Antennas*," IEEE International Symposium on Antennas and Propagation (APS), Puerto Rico, 2016.

- **Arslan Kiyani**, Raheel M. Hashmi and Karu P. Esselle, *"Performance Evaluation of Conventional and Planar Feeds in Resonant Cavity Antennas*," Advanced Electromagnetics Symposium, Malaga, Spain 2016.

Chapter 2

Resonant Cavity Antennas and Recent Progress

2.1 Overview

This chapter provides the basics of resonant cavity antennas (RCAs) along with different analytical models that have been used to study and explain their radiation mechanism. It also presents a generalized overview of the recent progress towards wideband RCAs. It should be remarked that the related literature is presented at the beginning of each chapter, accordingly.

2.2 Introduction

Resonant Cavity Antenna (RCA), also referred to as Electromagnetic bandgap resonator antenna (ERA), consists of an air-filled resonance cavity that is formed between a perfect reflector (eg., a metallic ground plane or an artificial magnetic conductor (AMC)) and a partially reflecting surface (PRS) [1–3]. Here we use the general term superstrate to refer to all such PRS. A highly reflective superstrate can significantly enhance the boresight directivity performance by reinforcing the radiated waves to undergo multiple reflections within the cavity [4, 5]. The typical configuration of an RCA is shown in Figure 2.1. It consists of a generic superstrate with thickness t and a metallic ground plane, which is separated by a distance h. Highly directive boresight radiation can be achieved using a single feed source,

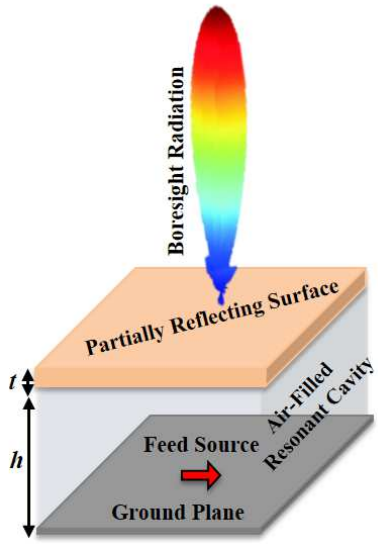

Figure 2.1: Typical configuration of a resonant cavity antenna with a generic superstrate/partially reflecting surface (PRS), a metallic ground plane and an example feed source

provided the cavity height h adjusted to satisfy the resonance condition [6].

2.3 Analytical Methods for RCA Characterization

Over the span of time, different analytical models were utilized to study the radiation behaviour of RCAs. These models can be categorized into following major groups: ray-tracing approximation [7, 8], transmission line model [6, 9, 10], EBG defect model [11, 12] and leaky wave model [13, 14]. Most of these models were mathematically complex and considered to provide less insight into the analysis of RCAs. Recently, more powerful and robust methods have been exploited based on periodic analysis approaches such as superstrate reflection model (SRM) and defect cavity model (DCM) [15]. All of these analytical models are based on certain assumptions to be applicable to different scenarios for the characterization of RCAs. However, rapid advancements in the computational power domain and availability of commercial simulation softwares (e.g. Ansoft HFSS, CST MWS, and FEKO, etc.) have laid the foundations for full-wave numerical analysis methods. In this thesis, all the design configurations of RCAs and RCA arrays have been conducted and carried out through full-wave software package of CST Microwave Studio.

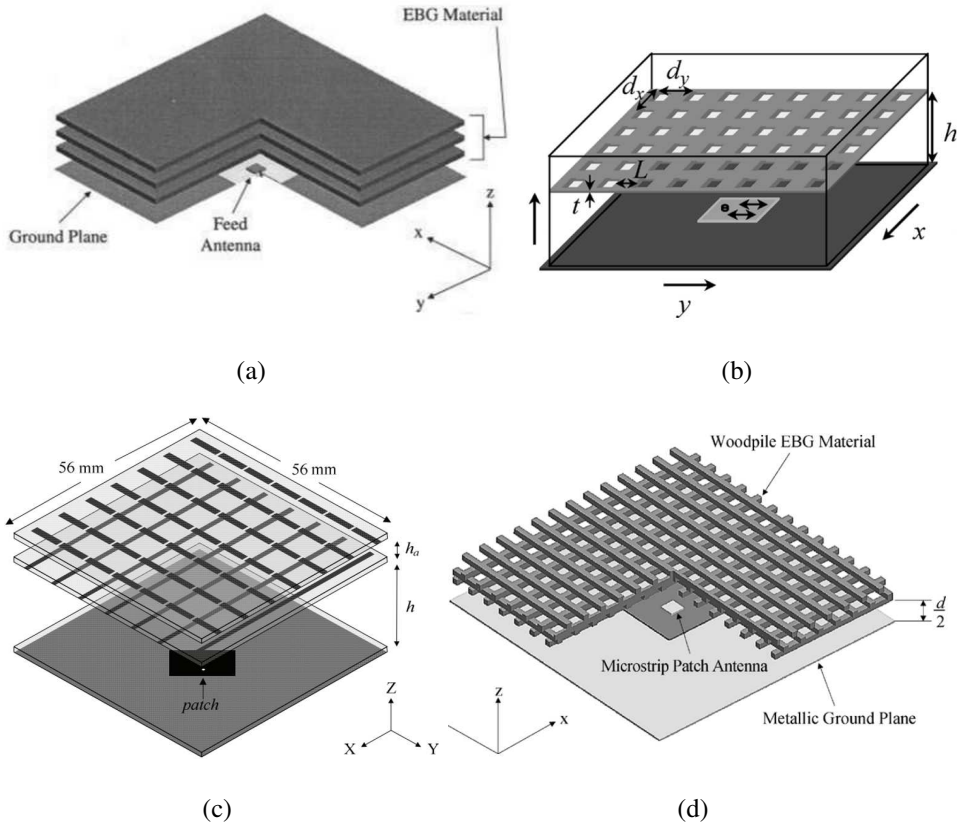

Figure 2.2: Schematics of RCAs with 1-D, 2-D and 3-D superstrates (a) 1-D stack of dielectric layers [3] (b) 2-D metallic grid [18] (c) 2-D FSS superstrate [21] (d) 3-D woodpile EBG superstrate [22]

2.4 RCA Superstrate Types

Superstrates are the most crucial design parameters for designing RCAs. The nature of superstrate has a significant role in achieving the highest boresight directivity and determining the directivity bandwidth of the resulting RCA. Directivity bandwidth is defined as the range of frequencies where the directivity of RCA remains within 3dB less than the maximum directivity value [16]. Superstrates are often classified in terms of dimensions, quantitatively, i.e. 1-D, 2-D or 3-D superstrates, whereas sometimes they are categorized structurally, qualitatively as printed and un-printed superstrates. They can be of various types, often formed by a 1-D stack of dielectric layers [3, 17], 2-D metallic superstrates and frequency selective surfaces (FSS) [18–21], or 3-D EBG structures [22, 23]. Some examples of RCAs with these superstrates are shown in Figure 2.2.

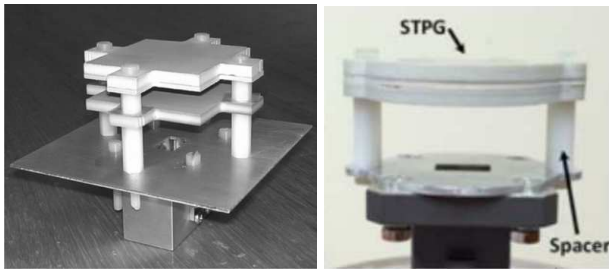

(a) (b)

Figure 2.3: RCAs with dielectric superstrates (a) composite superstrate with uniform permittivity [28] (b) superstrate with transverse permittivity gradient (TPG) [29]

2.5 Progress towards Wideband RCAs

Achieving highly directive boresight radiation by employing RCA configurations has been an attractive technique. It facilitates the design to construct relatively high gain antennas for use in various modern wireless communication applications. However, to achieve high gain, a strong superstrate reflectivity is required [8]. High superstrate reflectivity results in a highly selective resonant cavity (i.e. high Q-factor). Therefore, the resulting RCAs are highly directive but increasingly narrow-band. Owing to this, the design of wideband RCAs have attracted huge interest from many researchers in the present era, and continuous research has led to various commendable advancements in terms of their performance improvement.

Several RCAs have been proposed to address their narrow bandwidth behavior [20, 24–27]. These RCAs were excited using a single feed, shown to achieve the 3dB directivity bandwidth of 10-12% respectively. Although a single primary feed source is desirable to feed the cavity, sparse arrays and arrays of aperture-coupled slots have been demonstrated to improve the overall antenna performance with the 3dB directivity bandwidth of up to 13% alongside a peak gain of 19-20 dBi [10, 17]. However, the most significant advancements have been made recently by the introduction of all-dielectric composite superstrate and superstrate with transverse permittivity gradient (TPG) characteristics [28, 29]. They exhibited 3dB directivity bandwidth of 22% and 53% with a maximum peak directivity of 18.2 dBi and 16.4 dBi, respectively. The use of dielectric superstrates is attractive due to its symmetric nature, structure simplicity and ease of fabrication (as can be seen from Figure 2.3).

Chapter 3

RCA Element Selection for Array Implementation

3.1 Overview

A planar, single-layer dielectric resonant cavity antenna (RCA) is presented in this chapter. The RCA superstrate has a distinctive feature of having non-uniform permittivity in transversal plane. This configuration allows RCA to radiate efficiently with 3dB directivity bandwidth and 3dB gain bandwidth complementing each other. An excellent wideband matching response was obtained for the RCA with a -10 dB return loss bandwidth ranging from 20.96 GHz to 25.45 GHz. Numerical results predict a peak boresight directivity and gain of 18.7 dBi and 18.5 dBi respectively over a wide 3dB directivity bandwidth and 3dB gain bandwidth exceeding 49.31%. The wideband and highly-directive nature of this RCA element makes it suitable for RCA array configurations.

3.2 Introduction

RCAs have been widely investigated due to their planar configurations and highly-directive boresight radiation (often 15-20 dBi) [3, 30, 31]. Rigorous research has led to the design of simple RCAs, which employ dielectric-only superstrates. Recently, a new class of low-profile, extremely wideband RCAs have been proposed which uses single-layer, all-dielectric superstrates with transverse permittivity gradients (TPGS) [29]. RCA with TPG superstrate outperforms the RCA with uniform superstrates in terms of both peak directivity and directivity bandwidth. It uses a waveguide-fed slot as the feeding antenna and achieves a peak directivity of 16.5 dBi with a significant increase in the directivity bandwidth of 52.9%. In this chapter, we have designed a single-layer dielectric superstrate with TPG characteristics and optimized its performance for operation in 21.2 - 23.6 GHz frequency band[1]. This allows the selection of wideband RCA with excellent directive performance, particularly for the characterization of RCA Arrays.

3.3 RCA with TPG Based Superstrate (TPGS)

3.3.1 Design Configurations

For RCAs with TPG superstrate, classical design approaches based on unit-cell optimizations and or transmission line modeling are not suitable, as they assume uniform transverse extension to infinity. This limitation was overcome by conducting full-wave analyses to characterize the performance of the RCA. An exploded view of the proposed configuration of the RCA with TPGS is shown in Figure 3.1. All the dimensions and design parameters are optimized using parametric analysis. The design approach constitutes a circular superstrate with radius R and thickness t. The superstrate consists of three concentric segments with the highest permittivity in the centre and descending permittivity values towards the edges in such a way that $\varepsilon_a > \varepsilon_b > \varepsilon_c$. Each segment has a width w_i and relative permittivity of $\varepsilon_i (i \in \{2, .., N\})$, where N is the number of sections. A TPG can be obtained when all the segments have equal widths ($i.e. w_i = R/N$) and the permittivity of each segment is given by

[1] Allocated band for fixed wireless communication applications

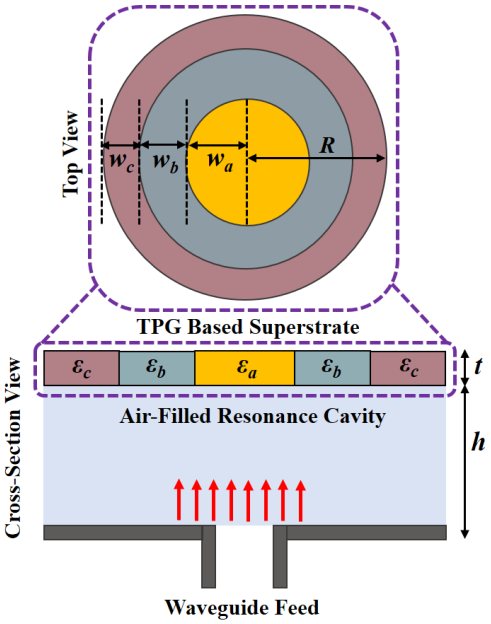

Figure 3.1: Design configuration of an RCA with TPG superstrate fed by a waveguide feed

$\varepsilon_{\mathrm{i}} = (i \times \varepsilon_{\mathrm{high}}/N)$. The radius R is $1.15\lambda_{low}$[2] and w_a, w_b and w_c are widths of sections in the superstrate, as shown in Figure 3.1 (each set to 11.1 mm). The superstrate sections are made out of Rogers TMM10i (ε_{a} = 9.8), Rogers RO6006 (ε_{b} = 6.15), and Rogers RO4003C (ε_{c}= 3.38) with the thickness t of each section set to 5.3 mm (i.e. $t = 1.2\lambda_{low}/(4\sqrt{\varepsilon_{\mathrm{a}}})$. The overall superstrate diameter is as small as $2.3\lambda_{low}$ and it is placed at a height $h \approx 0.5\lambda_{low}$ above the ground plane. It is important to emphasize that, for an RCA to radiate efficiently the 3dB gain bandwidth must be close to the 3dB directivity bandwidth. It can be accomplished by matching the antenna input to a standard 50Ωfeed-line over the entire 3dB directivity bandwidth. To serve the purpose, a waveguide-fed slot with the dimensions of $7.5mm \times 3.5mm$ was etched from the centre of the ground plane to form a feed antenna.

3.3.2 Numerical Results

Full-wave simulations were carried out in CST MWS to analyze the performance of proposed RCA element. Figure 3.2 illustrates the wideband and high-gain behavior of the RCA by depicting the input reflection coefficient ($|S_{11}|$) and boresight directivity performance of the TPGS. As shown in Figure 3.2, waveguide slotted feed is well matched over the entire frequency band of interest. The impedance bandwidth (bandwidth in which ($|S_{11}|$) remain

[2] λ_{low} is the wavelength at the lowest operating bandwidth

below -10 dB) extends from 20.96 GHz to 25.45 GHz (20%). Figure 3.2 also compares the boresight directivity and gain of the RCA. It can be seen that the TPGS demonstrates the peak directivity of 18.7 dBi and peak gain of 18.5 dBi respectively, with 3dB directivity bandwidth and 3dB gain bandwidth of 49.31%. This validates the fact that peak directivity and 3dB directivity bandwidth compliments the peak gain and 3dB gain bandwidth without any significant difference. Therefore, we use the terms peak directivity and 3dB directivity bandwidth throughout the thesis for consistency. The radiation pattern of the RCA at the center frequency of 22.4 GHz is plotted in Figure 3.3 for the two principal planes. The radiation patterns in E and H-Plane are inherently asymmetric in these type of antennas. It is evident that patterns are well directive and achieve low SLLs of -16.2 dBi and -18.9 dBi in both planes, respectively. The SLLs in H-plane were observed to be particularly better than E-plane.

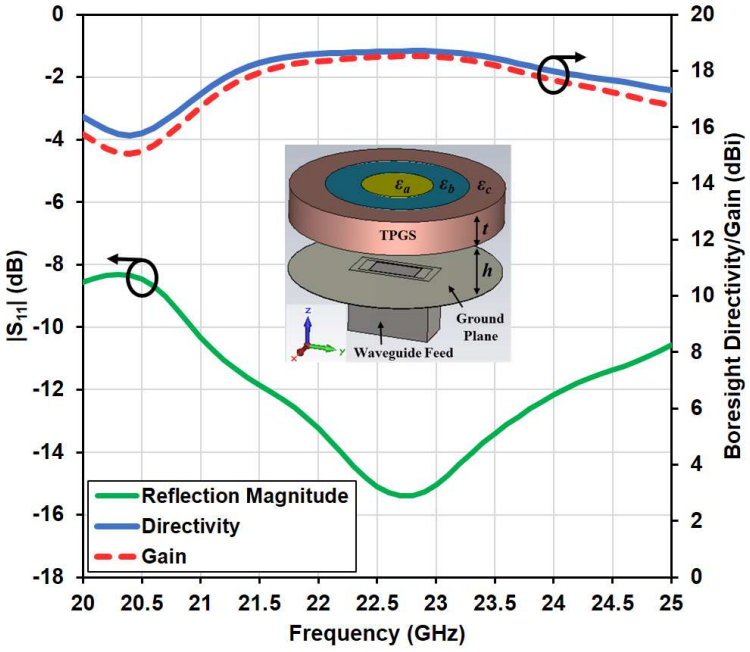

Figure 3.2: Performance of the RCA with TPGS (input reflection coefficient for $|S_{11}|$ below -10 dB and the comparison of boresight directivity and gain)

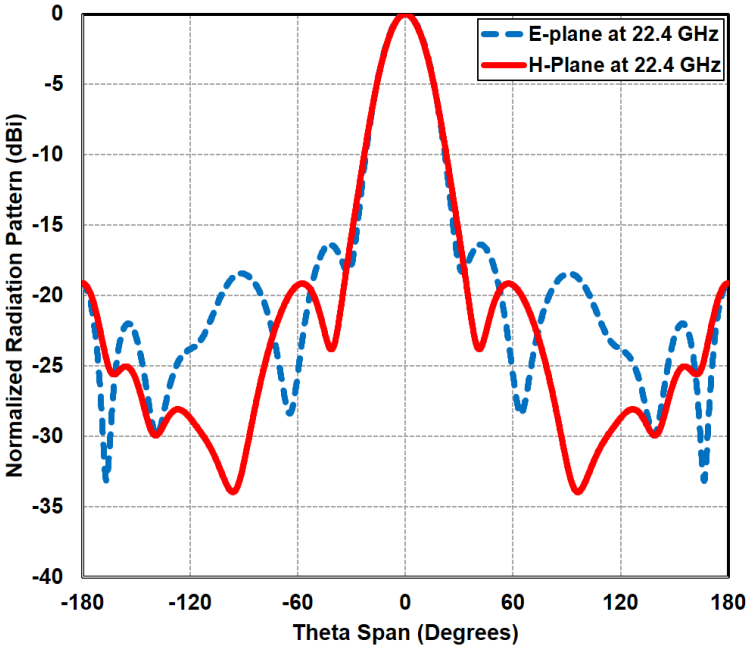

Figure 3.3: Normalized radiation pattern of the RCA with TPGS in two principal planes at the central frequency of 22.4 GHz

Chapter 4

Analytical Predictions and Array Topologies

4.1 Overview

Wideband and high-gain Resonant Cavity Antenna Arrays (RCAAs) are presented in this chapter. Array Factor (AF) predictions demonstrated the suitability of realizing such arrays with the TPG based RCA designed in Chapter 3. Next, two array topologies (comprising square & radial configurations) have specifically been studied thoroughly. The boresight performance is characterized on the basis of peak directivity, 3dB directivity bandwidth, and most importantly the far-field radiation pattern envelope (RPE) masks. In comparison to a 9×9 *square array, Tier7 radial array (having 91 elements) takes the shape of an HEX with a footprint area of* $28.3\lambda_{low}$ *x* $26.9\lambda_{low}$*. Numerical results are shown to achieve the peak directivity of 37 dBi with a 3dB directivity bandwidth of more than 20%. In addition, the proposed array demonstrated the potential of satisfying minimum ETSI Class-2 antenna requirements with appropriate RPEs and SLLs as low as -17 dBi.*

4.2 Introduction

Given the progress towards future smart-wireless communication systems, RCAs are being viewed as the emerging candidates for use in satellite reception, short-range to medium-range directional communications, as well as for various millimeter-wave applications. Certain applications, such as base station or backhaul antennas, require high gain along with stringent requirements to comply with radiation pattern envelopes (RPEs) as defined by standardization bodies such as ACMA[1]. In this context, several approaches have been considered to increase the gain of RCAs. An RCA with enhanced gain has been depicted in [10], where a multiple-layer high-permittivity superstrate was illuminated by sparse arrays as illustrated in Figure 4.1(a). The antenna achieved a gain of 19 dBi with the reasonable bandwidth of at least 5.7%. To improve the gain, an alternate approach which is based on the multipoint excitation of arrays has been introduced [17]. A dual-resonator 1-D EBG structure excited by 4×8 slot array feed (see Figure 4.1(b)) was presented to achieve the peak gain of 21 dBi along with the directivity bandwidth of 13%. Recently, a wideband sparse array made up of three dielectric layers based superstrate was proposed in [32]. The configuration of the sparse array by placing elements in close proximity demonstrated a peak gain of 21.3 dBi over a 3dB directivity bandwidth of 37%. However, all previous literature in this domain primarily focused on either increased directivity or widening the directivity bandwidth.

In this chapter, compact arrays of RCAs are studied with the primary goal of characterizing their radiation performance with respect to standard RPEs. We have designed and

[1]Australian Communications and Media Authority

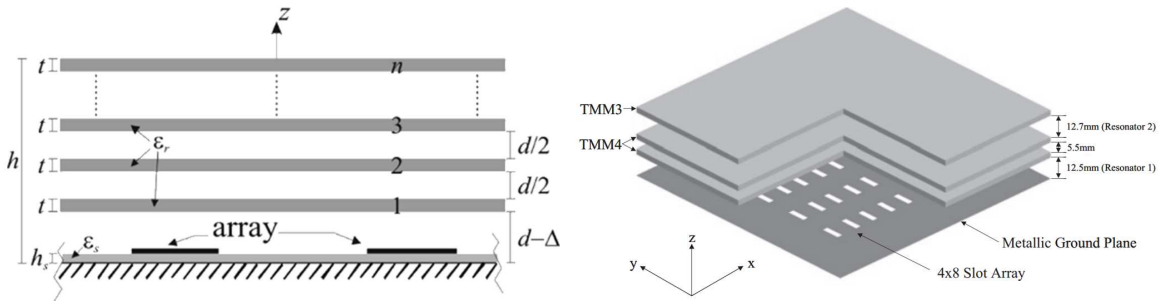

(a) (b)

Figure 4.1: Schematics of RCAs with (a) sparse array feed [10] (b) slotted-array feed [17]

rigorously investigated the square and radial array topologies to estimate the potential of planar configurations by achieving the high radiation performance with suitable RPEs.

4.3 Theoretical Array Factor Estimations

Fixed wireless communication applications (such as point-to-point communications) require performance to comply with radiation characteristics, as documented by the regulatory bodies. Initially, theoretical array factor (AF) calculations can provide useful insight into the far-field radiation characteristics before designing the actual RCAAs. These calculations have been performed using built-in array factor calculator in CST. It does not take into account the mutual coupling effect between array elements and the diffraction effect from the edges of the elements. However, the critical design parameters, such as number of array elements and the overall size of the array can extracted as an initial estimate.

4.3.1 Required Number of Array Elements and Inter-element Spacing

The CST based analytical AF approach is applied to estimate the number of array elements required to achieve the targeted peak directivity of 37 dBi. Predicted values of peak directivity corresponding to the number of array elements in square configuration are shown in Table 4.1. The single RCA element (designed in Chapter 3) achieves a peak directivity of 18.7 dBi for N=1. As, the number of array elements increase, the directivity increases gradually and reaches up to 37.7 dBi for N=81.

In the case of conventional arrays, the elements are spaced apart at a distance of $\lambda/2$ or more to avoid the mutual coupling effects and to increase the directivity. Thus, the effect of inter-element spacing is essential to study for the design of actual arrays. For RCAAs, the case of a 3×3 square array is considered here with elements in close proximity (S=2.3λ_{low}) and with elements spaced apart at a distance of $\lambda/4$, $\lambda/2$, $3\lambda/4$ and λ respectively. Theoretical AF estimations are then applied to quantify the relationship between the directivity performance and inter-element spacing, as illustrated in Figure 4.2. It offers a fast, simple way to calculate the far-field for an array Comparing the results in Figure 4.2, it can be seen that the array exhibited peak directivity of 28 dBi when elements are placed close to each other. While the highest peak directivity of 29.2 dBi is achieved, when the spacing between the array

elements is set to $3\lambda/4$. It is interesting to note that 3dB directivity bandwidth spans over the entire band with peak directivities ranging between 28-29 dBi for the each value of S. The peak directivity difference is not more than 1 dBi. This implies to the fact that by placing elements in close proximity as opposed to the conventional spacing of ($S = \lambda/2$), there is no significant reduction in the peak directivity. We can conveniently trade-off 1 dBi directivity for the compact array configurations with reduced footprint area.

Table 4.1: AF predictions for the required no. of array elements and the directivity values

No. of array elements (N)	**AF predicted directivity values (dBi)**
1	18.7
9	28.0
25	32.7
49	35.5
81	37.7

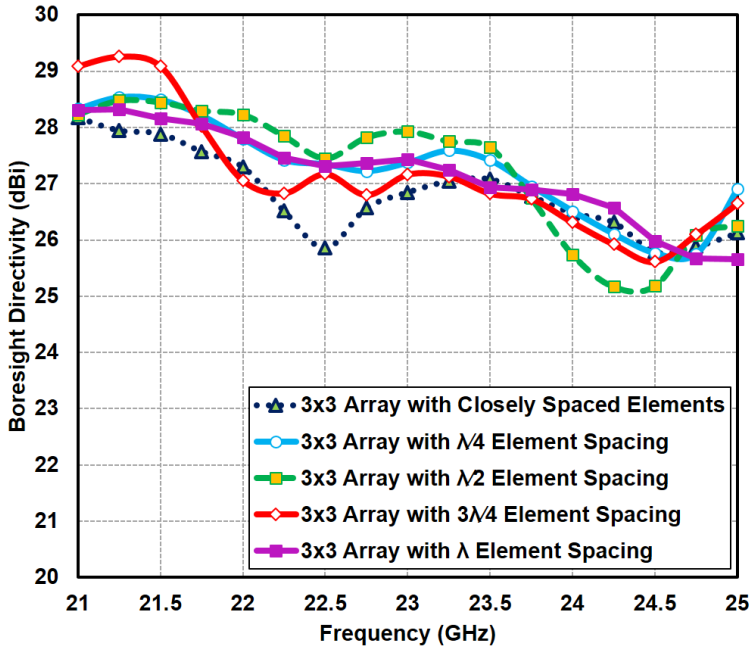

Figure 4.2: Array factor estimations for closely spaced elements and with the inter-element spacing of $\lambda/4$, $\lambda/2$, $3\lambda/4$ and λ

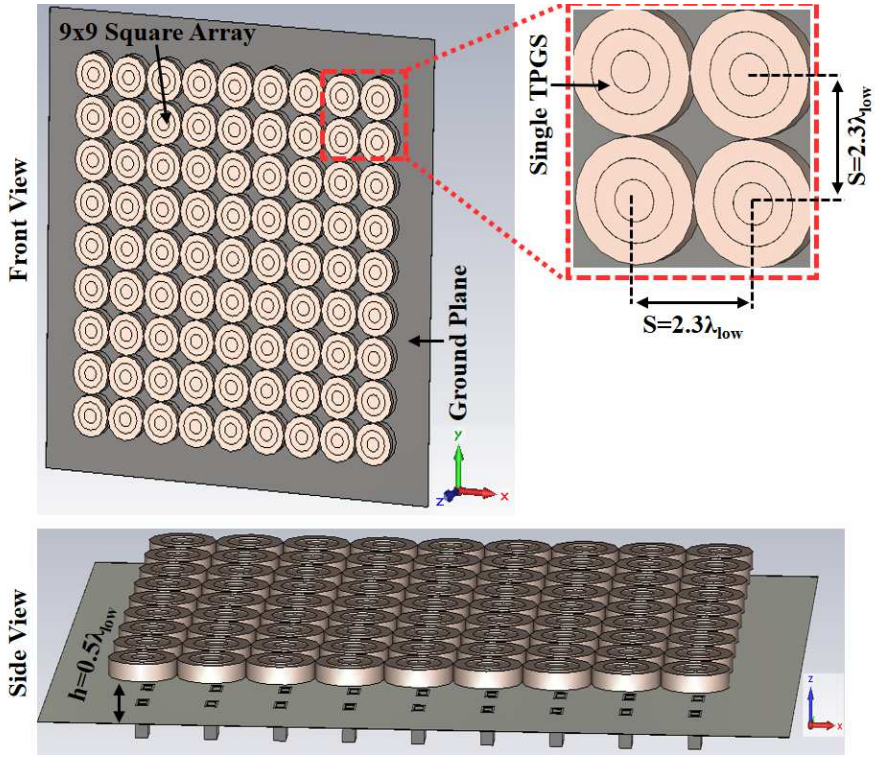

Figure 4.3: Design configurations of a 9×9 square array with closely spaced elements

4.4 Full-wave Analysis of RCA Arrays

Previously, array factor estimations have been carried out to study the theoretical array characteristics. Important considerations including the required number of array elements and the inter-element spacing between them have been discussed. The outcomes have provided the sound foundations to chalk out the design strategy for actual array simulations. With the primary objective to evaluate if the RCA arrays are able to meet the ETSI class-2 antenna requirements, full-wave analysis is used as it allows to consider the mutual coupling between the elements and also the edge effects. Two array topologies are studied in square and radial configurations.

4.4.1 9×9 Square Array

4.4.1.1 Geometrical Layout

The TPGS demonstrated and analyzed earlier in Chapter 3 is the main building block of the following array topology. It consists of a circular superstrate with three concentric rings. The

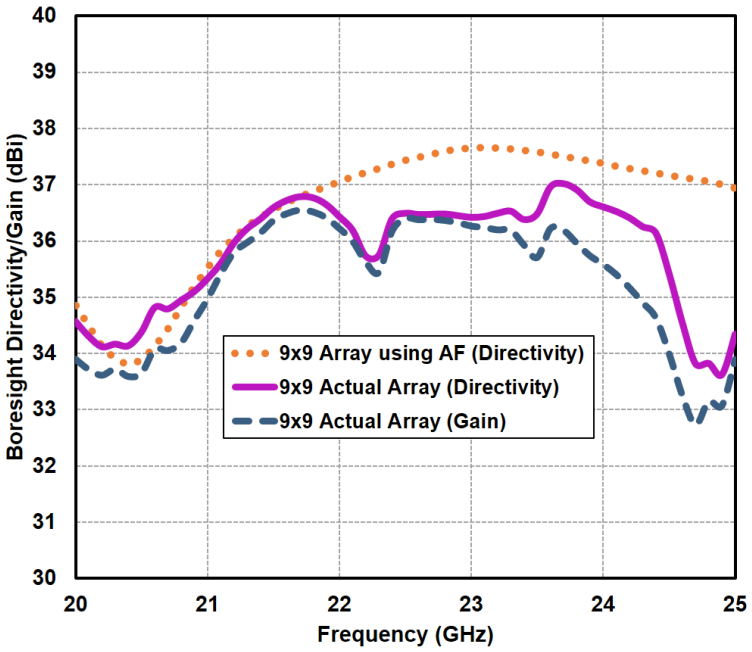

Figure 4.4: Comparison of predicted and computed directivity/gain of a 9×9 square array

thickness t of the each ring is set to 5.3mm with relative permittivity values of 9.8, 6.15 and 3.38 respectively. The superstrate is now employed to form an actual array of 81 elements, placed at the height of approximately $0.5\lambda_{low}$ above a common ground plane. The schematic of a 9×9 square array with closely spaced elements designed to operate within the targeted frequency band of 21.2 GHz - 23.6 GHz is presented in Figure 4.3. The overall footprint area of the square array is $25\lambda_{low} \times 25\lambda_{low}$. Each element is fed by the $7.5mm \times 3.5mm$ slot individually, which is excited using a WR-42 waveguide to coax adapter.

4.4.1.2 Numerical Results

Full-wave simulations of the 9×9 square array were carried out in CST Microwave Studio using the transient solver. Figure 4.4 compares the predicted and computed boresight directivity/gain of 9×9 square array. AF estimation curve as shown in Figure 4.4 predicted the achievable peak directivity of 37.7 dBi with the 3dB directivity bandwidth exceeding 20%. Moreover, the directivity response is quite flat and consistent throughout the band of operation. Whereas, full-wave analysis results in a peak directivity of 37 dBi and peak gain of 36.5 dBi, along with the 3dB directivity bandwidth and 3dB gain bandwidth of more than 20%.

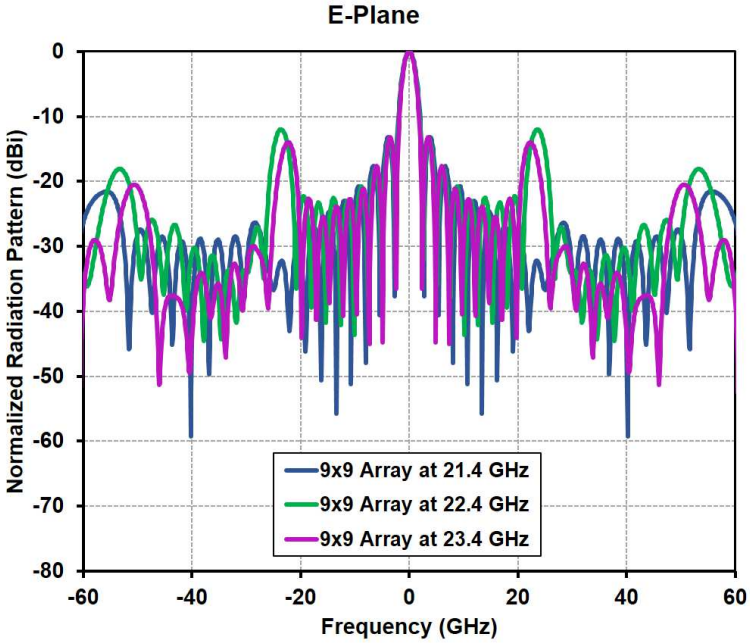

(a)

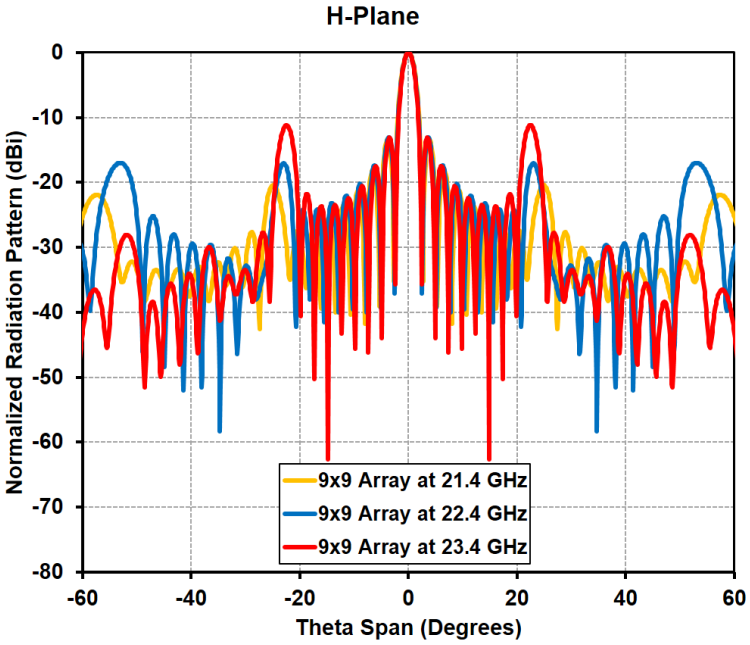

(b)

Figure 4.5: Normalized radiation patterns of a 9×9 square array (a) E-Plane at 21.4 GHz, 22.4 GHz, and 23.4 GHz (b) H-Plane at 21.4 GHz, 22.4 GHz, and 23.4 GHz

This validates the fact that peak directivity and 3dB directivity bandwidth compliments the peak gain and 3dB gain bandwidth without any significant difference. Comparing the curves in Figure 4.4, although the peak directivity and directivity bandwidth are adequate, the directivity fluctuates over the bandwidth as opposed to the prediction. This difference is due to the fact that AF estimations do not take into account the mutual coupling effects between the closely spaced array elements. Considering this, the overall directivity performance is found to be consistent with the AF predictions. This verifies the design procedure and demonstrates that the actual array can now be further investigated for far-field characterization.

The simulated radiation patterns of the 9×9 square array are shown in Figure 4.5. It can be observed that the E-plane and H-plane radiation patterns are computed for three different frequencies of 21.4 GHz, 22.4 GHz, and 23.4 GHz respectively. This gives a thorough insight into the behavior of patterns over the entire band. The radiation patterns appear to be directive with appropriate SLLs. The E-plane patterns attain consistent SLLs of -13.2 dB at the lower and higher frequency of 21.4 GHz and 23.4 GHz respectively. Whereas, the SLL at the central frequency of 22.4 GHz rises as high as -12 dB. On the other hand, H-plane depicted the minimum SLL of -13.3 dB at 21.4 GHz, which afterward rise to -11.2 dB at 23.4GHz, i.e., close towards the upper-frequency limit. It is interesting to notice that that the SLLs in both E and H-plane are closely related. Therefore, it can be concluded that the overall beam quality of the designed array structure is good with an average SLL of -13 dB in both principle planes.

RPE plots for the 9×9 square array are shown in Figure 4.6. The frequencies considered here are shown as 21.4 GHz, 22.4 GHz, and 23.4 GHz, which represent the lower, central and higher frequency within the directivity bandwidth. The standardized gain values of ETSI Class-2 antennas are mapped out at the particular azimuth angles of 5°, 10°, 20°and 50°, as delineated in Figure 4.6 (see the solid red lines). By taking it as a reference, the directivity values of the 9×9 square array are compared to various values of θ in both E and H-plane. Despite the fact that the 9×9 square array achieves the peak directivity of 37 dBi with moderate SLLs, Figure 4.6 depicts that it is still unable to meet the required radiation characteristics as set in ETSI Class-2 standards. The RPE inconsistency limits the practical use of such arrays, especially in applications with strict SLL requirements.

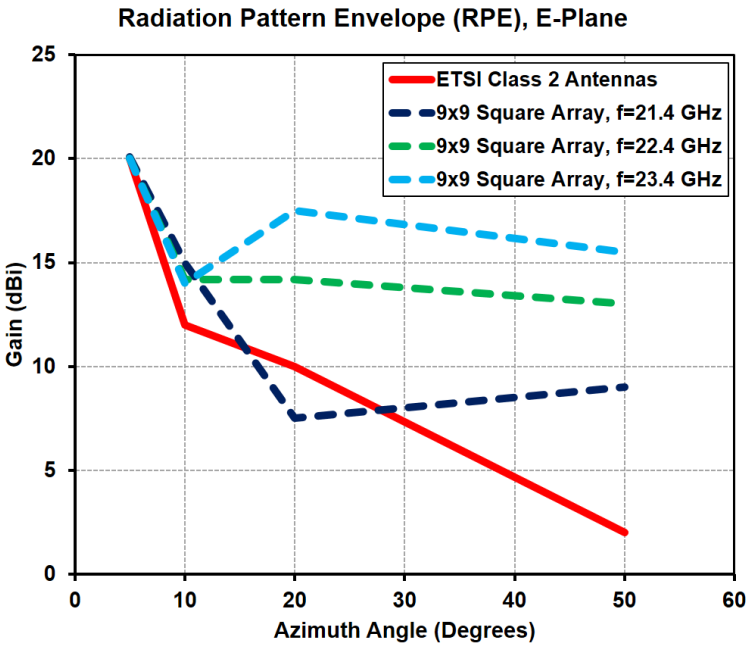

(a)

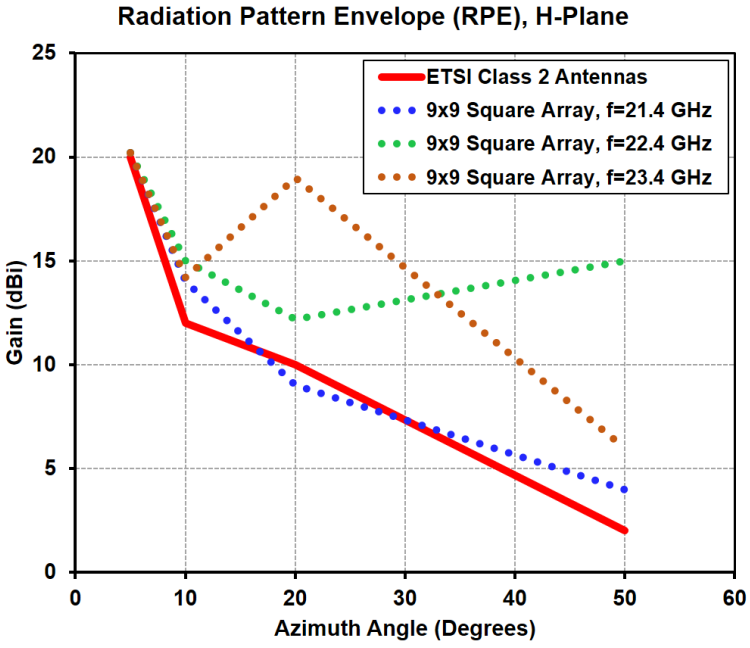

(b)

Figure 4.6: RPEs comparison of a 9×9 square array with ETSI Class-2 antenna (a) E-Plane at 21.4 GHz, 22.4 GHz, and 23.4 GHz (b) H-Plane at 21.4 GHz, 22.4 GHz, and 23.4 GHz

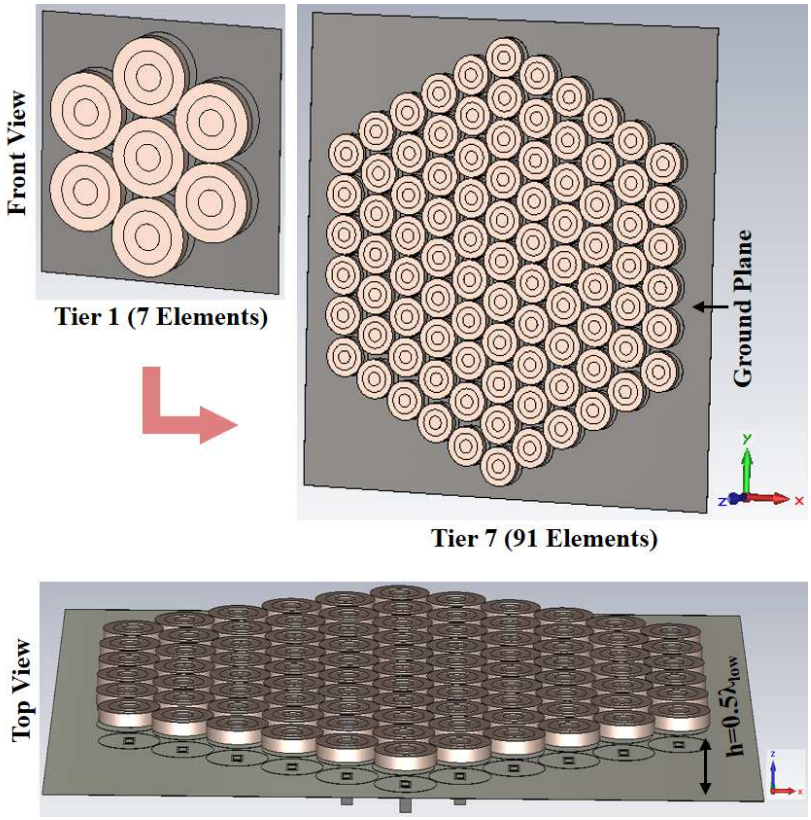

Figure 4.7: Design configurations of the radial array with 91 closely spaced elements

4.4.2 Tier7 Radial Array

4.4.2.1 Geometrical Layout

It is well known that one of the most important factors in shaping the array radiation pattern is the systematic placement of array elements. It is desirable to place elements in such a way that it increases the effective radiating aperture. To address this issue, we proposed a radial array in this section. All the design parameters are kept constant as mentioned before in section 4.4.1.1. Initially, a radial array with 7 elements (referred as Tier1) is designed by placing the array elements at the height of approximately $0.5\lambda_{low}$ above a common ground plane as shown in Figure 4.7. It is further extended to construct the Tier7 radial array comprising 91 array elements. The final configuration takes the shape of an HEX (see Figure 4.7). Each element is fed by the $7.5mm \times 3.5mm$ slot individually, which is excited using a WR-42 waveguide.

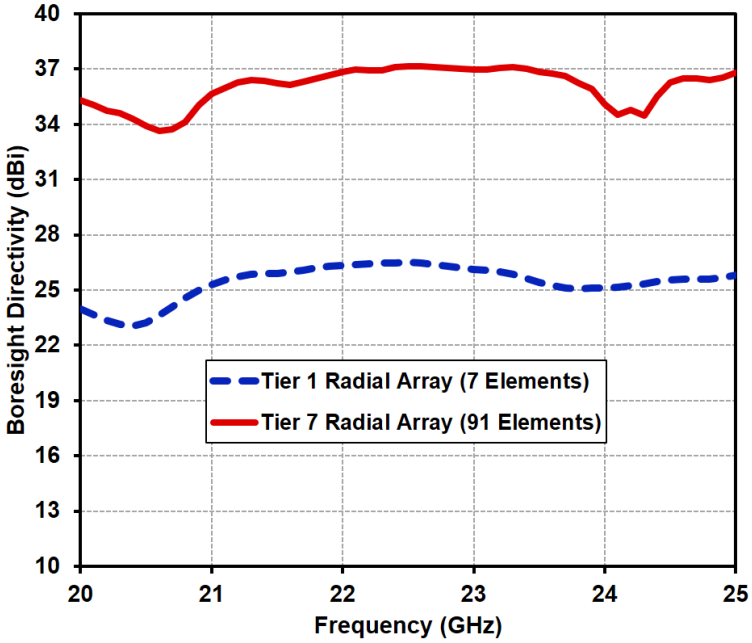

Figure 4.8: Computed boresight directivity of Tier1 and Tier7 radial arrays

4.4.2.2 Numerical Results

Figure 4.8 shows the computed boresight directivity of Tier1 and Tier7 radial arrays, respectively. The Tier1 radial array has a peak directivity of 25 dBi with 3dB directivity bandwidth covering the entire frequency band of interest. Similarly, the maximum computed peak directivity of 37 dBi can be seen in Figure 4.8 for the Tier7 radial array. Its 3dB directivity bandwidth is greater than 20%, i.e., extends over the entire targeted band. After achieving the desired directivity performance, the main focus now lies on investigating the influence of HEX configuration on the resulting RPEs.

Recorded radiation patterns for Tier7 radial array at three different frequencies are plotted and compared in Figure 4.9. The frequencies 21.4 GHz, 22.4 GHz and 23.4 GHz, are considered to cover the whole operational band. Figure 4.9 illustrates the significant improvement in terms of radiation performance. It is evident that the Tier7 radial array with HEX configuration achieves well-directed pencil beam with low SLLs, as compared to the 9×9 square array. The E-plane radiation patterns exhibit comparatively low SLLs. They remain close to -17 dB at the starting frequency of 21.4 GHz and fall to -19 dB and -19.5 dB towards the central and upper-frequency limit, respectively. The H-plane, on the other hand, depicts the

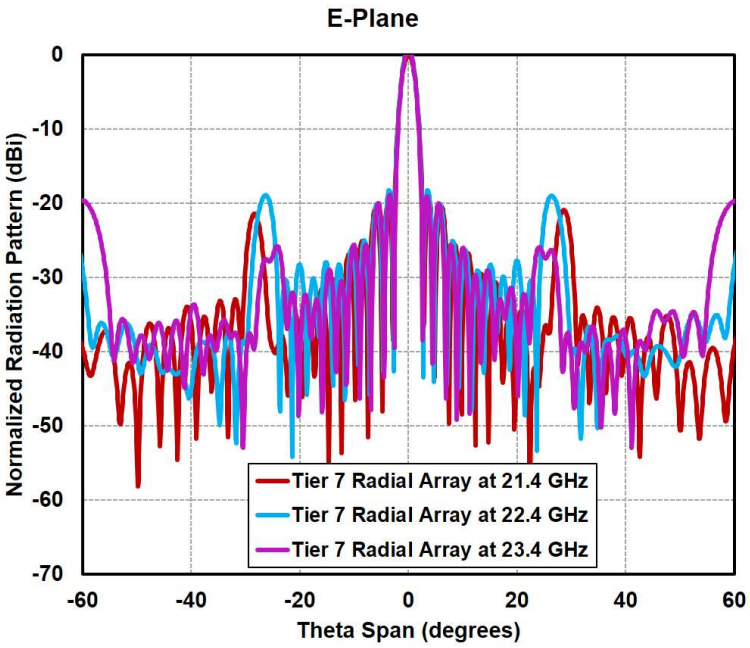

(a)

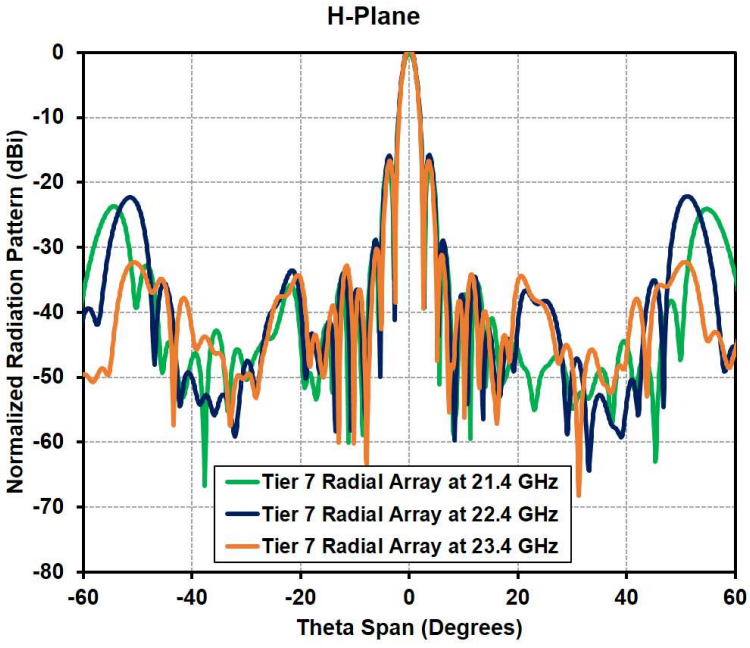

(b)

Figure 4.9: Normalized radiation patterns of the Tier7 radial array (a) E-Plane at 21.4 GHz, 22.4 GHz, and 23.4 GHz (b) H-Plane at 21.4 GHz, 22.4 GHz, and 23.4 GHz

stable SLLs of approximately -16.5 dB at the lower frequencies and reach down to -17.4 dB at the higher frequency of 23.4 GHz.

RPEs for Tier7 radial array at 21.4 GHz, 22.4 GHz, and 23.4 GHz are shown in Figure 4.10. The directivity values are plotted at azimuth angles of 5°, 10°, 20°and 50°respectively. Now, let us compare the performance of proposed Tier7 radial array with the ETSI Class 2 antenna RPEs (represented by solid red lines in Figure 4.10). For Tier7 radial array, the E-plane completely followed the envelope trend. The directivity values for all the frequencies showed good agreement at each of the objective angles. On the other hand, the H-Plane traced the envelope for lowest frequency of 21.4 GHz. However, the directivity values for central and upper frequencies of 22.4 GHz and 23.4 GHz remained consistent only at 5°, 10°and 20°before increasing above the standard gain value at 50°. The overall RPE characteristics of Tier7 radial array are attractive as they have displayed the potential to approach Class-2 antenna requirements reasonably.

4.5 Discussion

In this chapter, we have thoroughly investigated two different array topologies. Therefore, it is essential to address the tradeoff between both array configurations and their radiation characteristics. Since, the arrays were fed using waveguide feeds, the input impedance of individual elements is similar to the input impedance of an isolated RCA. It is important to note that the array radiation patterns demonstrate grating lobes at about 25°, caused by the large inter-element spacing. The reason these lobes change in the H-Plane between the square array and Tier7 radial array is because the spacing between the elements change in the H-Plane. The E-Plane spacing is constant between the two arrays. However, comparing the directivity performances of both arrays from Figure 4.4 and Figure 4.8, one can notice that the Tier7 radial array has consistent and much flatter response over the directivity bandwidth. Tier7 radial array not only achieves the lower SLLs than 9×9 square array, but also showcased the capability of generating appropriate RPEs suitable for commercial applications.

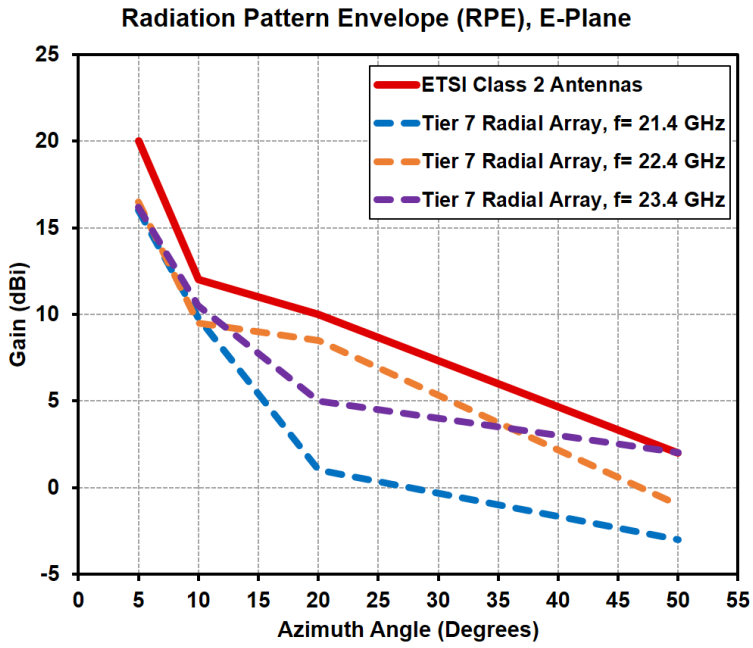

(a)

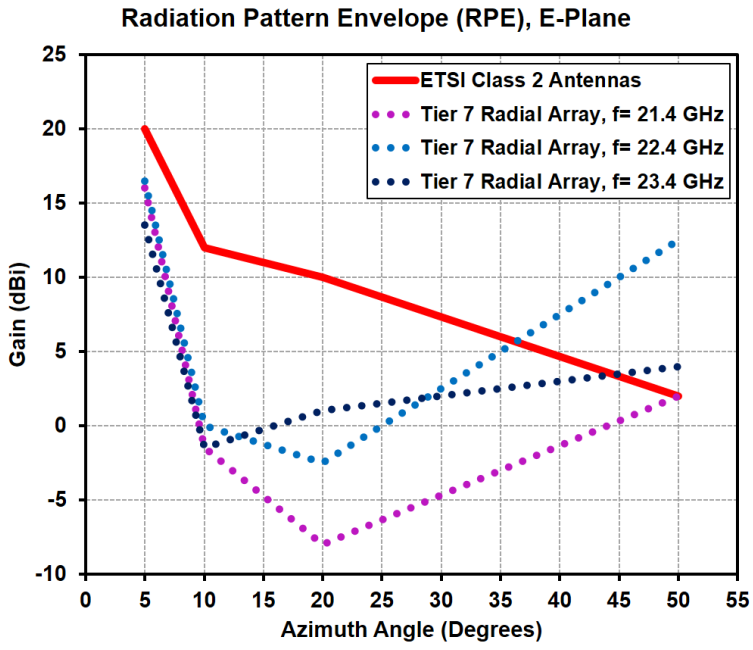

(b)

Figure 4.10: RPEs comparison of a Tier7 radial array with ETSI Class-2 antenna) E-Plane at 21.4 GHz, 22.4 GHz, and 23.4 GHz (b) H-Plane at 21.4 GHz, 22.4 GHz, and 23.4 GHz

4.6 Conclusion

A new class of simple and planar wideband arrays has been proposed and studied thoroughly. Two array topologies based on square and radial array configurations were investigated. Tier7 radial array showcased the ability to satisfy ETSI Class-2 antenna specifications among both configurations. Numerical results demonstrated high-directivity and wide directivity bandwidth covering the entire targeted band. It is shown to achieve the peak directivity of 37 dBi with a 3dB directivity bandwidth of more than 20%. In addition, the array has a significant advantage of reduced footprint area with elements in close proximity. The compact structure and low-profile characteristics of such arrays make them highly suitable for directive point-to-point applications.

Chapter 5

Investigation on SLL Reduction Using a Dielectric Phase Correcting Structure

5.1 Overview

An all-dielectric phase correcting structure (PCS) is investigated to improve the radiation characteristics of Resonant Cavity Antenna Arrays (RCAAs). By using the 3×3 *square array, a thorough analysis of the aperture phase distribution is studied and presented in this chapter. Furthermore, it brings out the detailed procedure for the design and implementation of PCS. Far-field results of directivity and SLL are then compared with and without PCS by addressing the aperture phase transformation. Numerical results demonstrated a slight improvement of 0.6 dBi in the peak directivity and 1.8 dBi reduction in the SLL at the operating frequency of 22.3 GHz. This feature can be effective, particularly for the design of sparse arrays. Finally, the chapter concludes by suggesting a few methods to attain significant performance enhancement.*

5.2 Introduction

RCAs have demonstrated excellent potential for use in modern wireless technologies. With the recent advancements in communication systems, many practical applications demanded antennas to satisfy stringent criteria of achieving high directivity and reduced side lobe levels (SLLs). SLL reduction plays a significant role in the antenna pattern synthesis. It is considered as one of the crucial factors to shape the RPEs. However, recent research investigations have revealed that the aperture phase distribution on the classical RCAs is highly non-uniform resulting in poor radiation performance such as low directivity and high SLLs [33]. It has been demonstrated that the phase correcting structures (PCS) can significantly improve their radiation properties. The idea of phase correction has been extended to improve SLL of RCAA which is explained in this chapter.

5.3 Phase Correcting Structures (PCS)

Traditionally lenses have been used to improve radiation performance through enhanced phase uniformity. The designs were based on dielectric-plano-hyperbolic lenses (DPHLs), Fresnel lenses and Fresnel zone plates [34, 35] which were later replaced by flat all-dielectric permittivity varying and planar printed lenses [36, 37]. All of the traditional lenses are based on ray-optics. They are usually fed by the antennas that are approximated by a point source located at the focal point of the lens. However in case of RCAs, we have a non-uniform feed source at the back which doesn't allow the point source approximation due to the resonance and multiple reflections in the cavity. This rules out the traditional lenses adaptation for the phase correction of RCAs. Therefore, an all-dielectric PCS has been realized for RCAs in [38]. The reported technique determines the phase error by using full-wave simulations rather than ray-optics. By applying PCS, a significant improvement in radiation performance was observed which includes higher gain, lower side lobe levels and better aperture efficiency.

Although method has been demonstrated for single RCA, no attempt has yet been made to improve the aperture phase distribution of RCAAs by applying this technique. In this research work, we comprehensively investigated and implemented the PCS to observe the radiation performance of RCAAs. The primary objective of this study is to explore the possibility of improving the directivity performance and reducing the SLLs of RCA arrays.

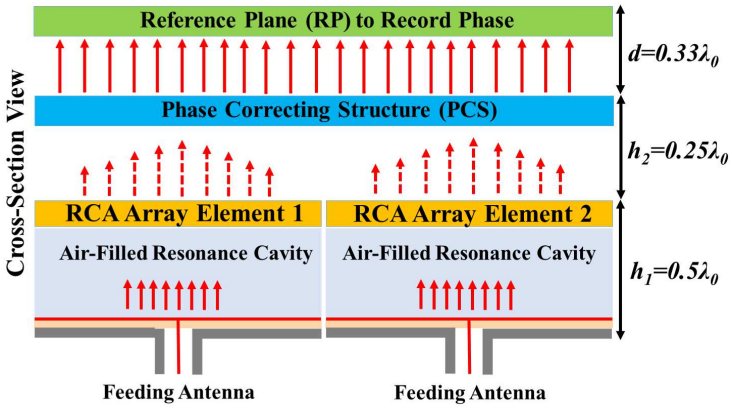

Figure 5.1: Design configurations of RCAA elements with phase correcting structure (PCS)

5.4 PCS Operation Principle

The proposed configuration of the RCA array elements with a PCS is presented in Figure 5.1. In order to clearly demonstrate the phase correction concept, the example structure considered here consists of two waveguide-fed RCAs. The two RCA array elements are identical and placed side by side, having the cavity height h_1 of $0.5\lambda_{low}$. The PCS is shown to be placed at a distance h_2 of $0.25\lambda_{low}$ above the two RCA array elements. This surface is required to handle all the waves radiating out of the cavity along with the side waves leaving the cavity in lateral dimensions. Finally, a reference plane (RP) is set at a distance d of $0.33\lambda_{low}$ to record the output phase. It should be noted that the value of h_2 has been taken as a reference from dielectric RCAs with three superstrates separated apart by the classical quarter guided-wavelength value [3]. Whereas, the value of d can be adjusted based on the required phase range for correction as explained in [38].

5.4.1 Near-field Distribution

To study the performance in terms of aperture phase distribution, a deeper insight into the near-field radiation is required. For this purpose, a 3×3 square array is considered here instead of a very large array due to computational limitations; the array is shown in Figure 5.2. The array elements are placed at the height of $0.5\lambda_{low}$ above the ground plane. The waveguide-fed slot (with dimensions 10.7×4.3 mm) in the ground plane is used as the feeding antenna for each element separately.

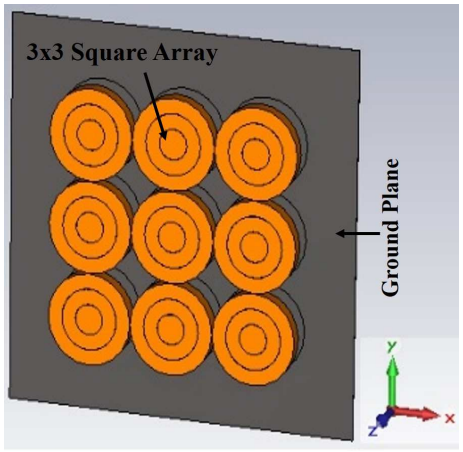

Figure 5.2: A perspective view of a 3 × 3 RCAA. The array has a common ground plane

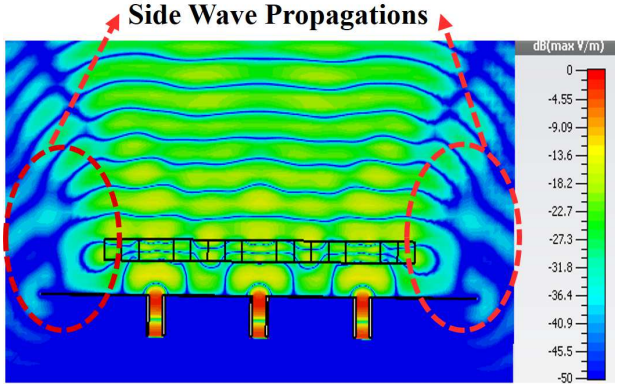

Figure 5.3: E-Plane phase distribution of a 3 × 3 RCAA

Full-wave simulations were carried out to understand the aperture phase distribution of the RCAA. The phase of radiated electric field is examined at the height of approximately $0.25\lambda_{low}$ above the array. The cross-section of RCAA with field map is presented in Figure 5.3. It can be seen from the Figure 5.3 that the phase distribution is quite symmetrical, and it is not significantly deteriorated in comparison to the classical RCAs, as demonstrated in [39]. This is due to the fact that the elements of the array radiate coherently from multiple points leading to the synchronous aperture field. However, the strong side wave propagations towards the edges can be witnessed from Figure 5.3. The generation of side waves can lead to deteriorating the overall radiation performance and may contribute to side lobes. Therefore, it is essential to take into account the effect of these side wave propagations.

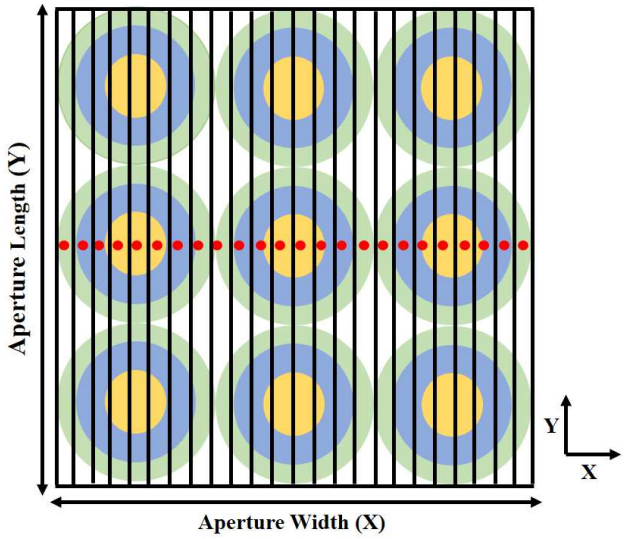

Figure 5.4: Physical aperture of a 3×3 RCAA with 26 discrete points (represented by red dots)

5.4.2 Aperture Phase Recording Technique

Although the phase distribution was observed in whole aperture of the array but as a proof of concept, phase correction was only attempted in E-plane. To do so, the physical aperture of a 3×3 square array is discretized into 26 equal columns each of width $0.33\lambda_{low}$ as shown in the Figure 5.4. The phase (E_x) of the electric field is recorded at the discrete points at the center of parallel columns. The phase values obtained from these discrete points are used to determine the phase delay required in each column. The required phase delay is actually the difference of phase between the PCS input and reference plane output, as given by $\phi_T = \phi_{PCSinput} - \phi_{RPoutput}$. This phase delay is implemented by appropriately changing the height of the PCS in a particular column. Consequently, the required height of the dielectric material can be determined by the total phase delay, which can be calculated by using equation 5.1 [38].

$$\phi_T(h_n) = \tan^{-1}\left(\frac{1+\epsilon_r}{2\sqrt{\epsilon_r}}\tan(k_n h_n)\right) + k_0(d - h_n) \tag{5.1}$$

$$\text{where } k_0 = 2\pi/\lambda_0; k_n = k_0/\sqrt{\epsilon_r}$$

Equation 5.1 represents ϕ_T, the total phase delay as the function of dielectric height h_n. Where k_o is the wave number in air. k_n is the wave number in dielectric and d is the distance between the PCS and RP. The phase of E_x, dominant field component, recorded earlier at the centre of discrete points is given in Table 5.1. It can be seen from Table 5.1 that the phase values get mirrored after 7th column due to phase symmetry in E-plane. The minimum and maximum phase value are shown to be -40°and 90°respectively. It depicts that the PCS requires to compensate the phase of around 130°. The total phase of the PCS is then calcualted ($\phi_T = \phi_{PCSinput} - \phi_{RPoutput}$) by setting the required phase at RP_{output} to -140°(less than the minimum normalized phase).

Table 5.1: Phase of the electric field generated by 3×3 RCAA in the E-Plane

Column No.	**Center Position of Discrete Points (mm)**	**Phase at Discrete Points (degrees)**	**Normalized Phase (degrees)**	**Phase Delay (degrees)**	**PCS Height (mm)**
1	-33.21	-40	-130	9	0.5
2	-5.52	70	-21	119	10
3	22.18	81	-9	130	10.7
4	49.87	58	-32	108	9.3
5	77.57	90	0	140	11.3
6	105.26	73	-17	123	10.3
7	132.96	68	-22	118	9.9
8	160.65	73	-17	123	10.3
9	188.35	90	0	140	11.3
10	216.04	58	-32	108	9.3
11	243.74	81	-9	130	10.7
12	271.43	70	-21	119	10
13	299.13	-40	-130	9	0.5

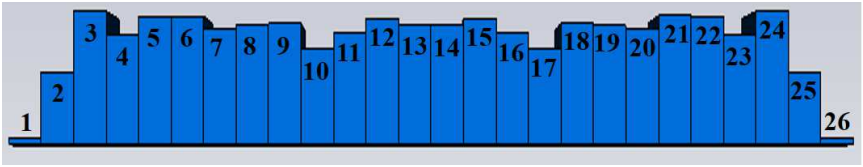

Figure 5.5: Cross-sectional view of PCS (with 26 segments)

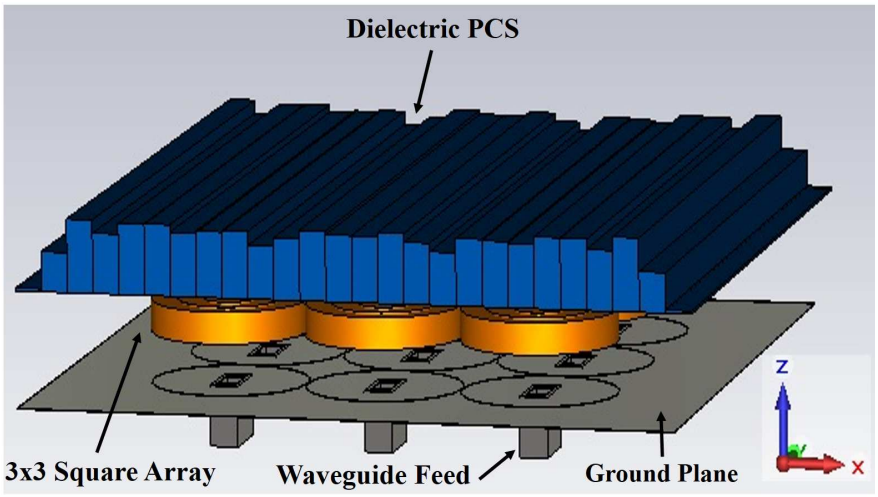

Figure 5.6: Design configuration of a 3×3 RCAA with PCS

5.4.3 PCS Design and Implementation

To design the PCS, choice of suitable dielectric material is critical. Careful considerations have been put forth to select the appropriate dielectric material. It is worth mentioning that a low permittivity material tends to increase the height of the PCS whereas, a high permittivity material will result in the increased internal reflections from PCS towards the array elements. Therefore, in this case Rexolite material with relatively low permittivity value of ($\varepsilon_{\mathrm{r}} = 2.53$) was utilized to serve the purpose. By substituting the specific values of ε_{r} and d in equation 5.1, a database was generated in MATLAB to obtain the desired height of each PCS segment, as summarized in Table 5.1. The cross-sectional view of resulting PCS is presented in Figure 5.5. Finally, the generated PCS was placed above the RCAA at the distance h_2 of $0.25\lambda_{low}$. A full design configuration of 3x3 RCAA with PCS is shown in Figure 5.6.

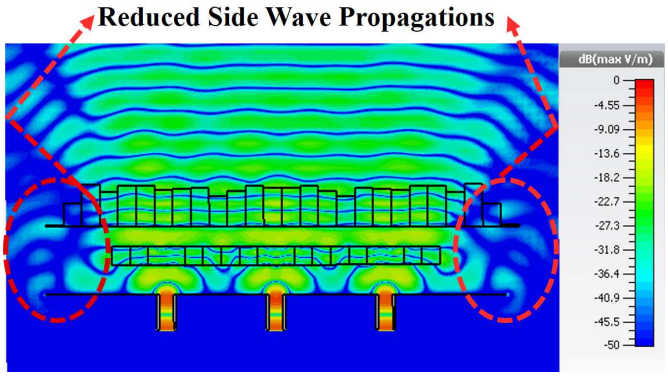

Figure 5.7: E-Plane phase distribution of a 3×3 RCAA with PCS

5.5 Numerical Results and Discussion

Full-wave simulations for the integrated antenna structure with 3×3 square array and the PCS shown in Figure 5.6 were conducted in CST Microwave Studio. To demonstrate the aperture phase distribution, the field map of E_x propagation is depicted in Figure 5.7. By comparing the phase with and without PCS, it can be seen that that the lateral width of uniform phase region extended slightly. However, the addition of PCS has no significant impact on the overall phase distribution. On the contrary, it is evident that the PCS has notably reduced the side wave propagations (see highlighted region with dotted red circles in Figure 5.7). This is due to the fact that low permittivity Rexolite material compensates the phase delay for lateral propagations towards the cavity edges. Further investigations into the far-field performance revealed that the introduction of PCS depicts varying directivity response within the operating band as shown in Figure 5.8. The variation in the peak directivity with the increase in frequency corresponds to the relatively less uniform surface phase at the starting frequencies and relatively more uniform surface phase at the central and higher frequencies. Let us compare the directivity and SLL values at the operating frequency of 22.3 GHz. It can be observed from Figure 5.8 and Figure 5.9 respectively that the peak directivity increased from 27.2 to 27.8 dB with the SLL reduction of 1.8 dB in E-Plane.

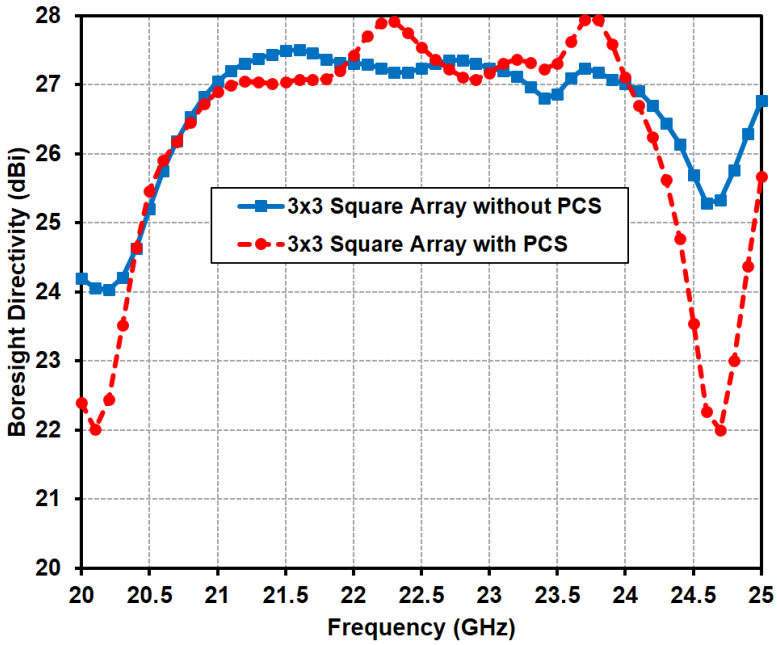

Figure 5.8: Directivity comparison of a 3×3 RCAA with and without PCS at the operating frequency of 22.3 GHz

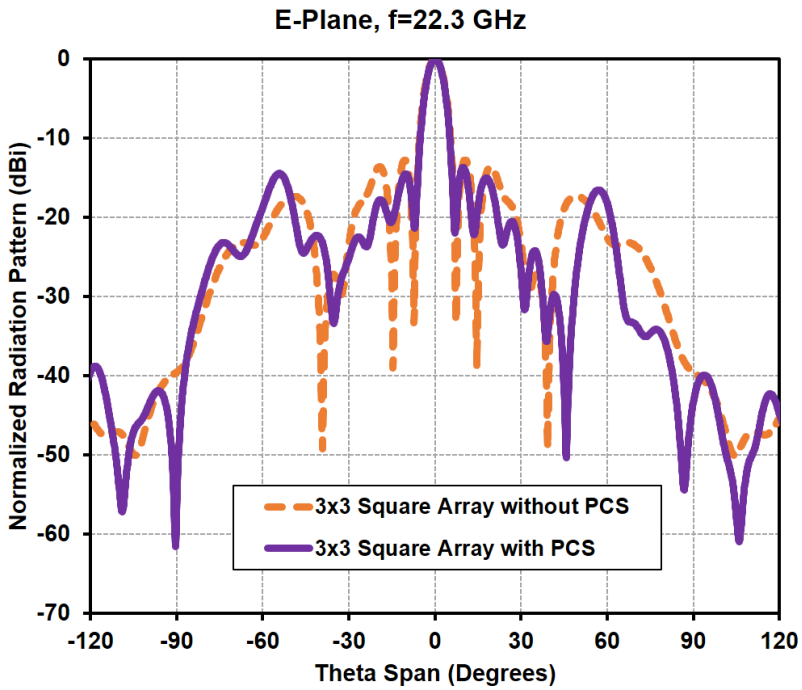

Figure 5.9: Radiation pattern comparison of a 3×3 RCAA with and without PCS at the operating frequency of 22.3 GHz

5.6 Conclusion

A dielectric PCS is implemented and investigated to improve the radiation characteristics of RCAAs. Unlike in the case of RCAs, directivity improvement of RCAAs is not significant due to PCS because the phase distribution of RCAA is a lot more uniform that that of a conventional RCA (with one slab superstrate made out of the same dielectric) even without the PCS. For low side-lobes, uniform aperture phase distribution is not the optimal distribution. For example, a cosine phase distribution was found to better. Amplitude distribution can be tapered, by feeding elements with different amplitudes, to reduce side-lobe level first. Then a phase correction surface can be added to re-shape the phase distribution to an optimal distribution.

Chapter 6

Scalable Planar Feeding Techniques for Array Applications

6.1 Overview

Simple and planar feeding techniques are evaluated for use in wideband Resonant Cavity Antennas (RCAs). Boresight directivity performance of the planar (aperture-coupled single slot/aperture-coupled dual slot) and a conventional feeding antenna (waveguide-fed slot) are investigated by placing each under an unprinted all-dielectric single-layer superstrate with transverse permittivity in lateral dimensions. An excellent wideband matching response was obtained for the RCA with a -10 dB return loss bandwidth ranging from 20.81 to 25.32 GHz. Numerical results predict a peak boresight gain of 17 dBi over a wide 3dB directivity bandwidth of 16.2%. The use of this planar, printed feed antenna reduces the overall height of the RCA and is easily extendable. This type of planar feeding configuration is well-suited for scalable RCA configurations such as sparse arrays or switched-polarization arrays with printed feed networks.

6.2 Introduction

RCAs have evolved as the emerging candidates for their extended use in modern space communications, various millimeter-wave applications and particularly in fixed radio communication systems. To achieve a wide 3dB gain-bandwidth in RCAs, it is imperative that the 3dB directivity-bandwidth of a particular RCA (associated with the superstrate) is complemented by an equally wide impedance bandwidth (associated with the feed). Therefore, the design of an appropriate and well-matched feed antenna is crucial to obtain the optimized RCA performance for practical applications. Moreover, the implementation of feed network distribution is quite challenging especially in the case of RCAAs with a large number of elements.

6.2.1 RCAs with Waveguide Feed Antennas

Rigorous research has led to the development of simple and wideband RCAs, which are capable of achieving directivities in the range of 15-20 dBi with excellent bandwidth exceeding 20% [28, 40, 41]. Most of the wideband RCAs proposed recently rely on waveguide-based feeds as shown in Figure 6.1. Waveguide-fed slot antennas fall into the category of commonly used RCA feeds, since they attribute low-loss and support a wide bandwidth of operation. Despite excellent performance of these wideband RCAs, a major limitation prevails is their feeding mechanism. RCAs with waveguide feeds are very expensive, especially when used to design arrays. Therefore, planar feeding methods while achieving comparable performance are invaluable to the design of RCAAs.

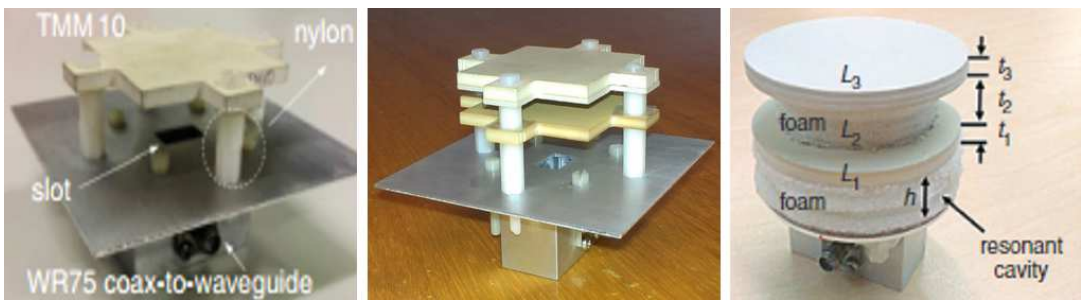

Figure 6.1: Recently developed wideband RCAs with waveguide feeds [27, 39, 40]

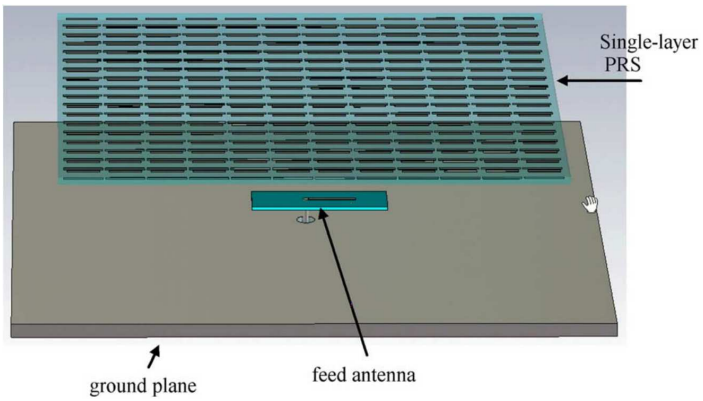

Figure 6.2: Cross-section of RCA with suspended monopole feed antenna [26]

6.2.2 RCAs with Planar Feed Antennas

Microstrip patch antennas are known for their distinct features of being planar, small size, light weight, low cost and easy to fabricate. Other key features are their conformability and ease of integration with various active components and RF devices. Owing to these benefits, microstrip antennas stand out for various microwave and engineering applications involving the printed circuit technology [42].

In the past few years, microstrip antennas with the transmission line and aperture-coupling techniques have gained attention to be employed as the feeding antennas for RCAs. In this context, two different approaches have been reported in [27, 43] for different superstrates. The first one demonstrated a thin PRS surface to design a wideband EBG resonator antenna. The superstrate is composed of a single dielectric slab with two-dimensional dipole arrays printed on both sides as shown in Figure 6.2. A probe-fed monopole antenna is suspended parallel to the ground plane to excite the cavity. Experimental results depicted an impedance bandwidth of 12.6% with a peak gain of 16.2 dBi and 3dB gain bandwidth of 15.7%.

The second approach proposed a double layer dielectric superstrate. It employed a slot-coupled patch antenna to achieve a wide impedance bandwidth. Figure 6.3 shows the configuration of both the superstrate and the feeding antenna. The suspended parasitic patch antenna excites the cavity when coupled by feed-line through the slot in the ground plane. By combining the superstrate and the feeding antenna, broad bandwidth response of 25.8% is achieved with the peak gain of 15 dBi.

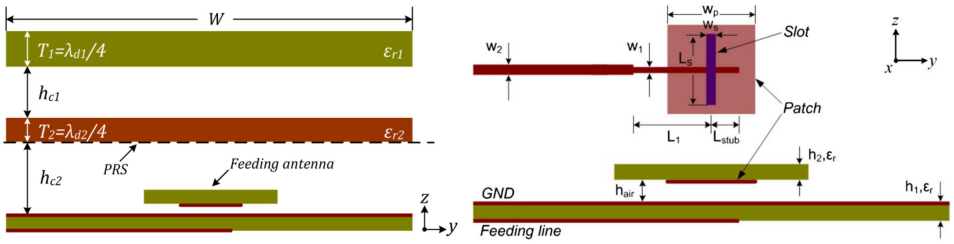

Figure 6.3: Cross-section of RCA with slot-coupled patch feed antenna [42]

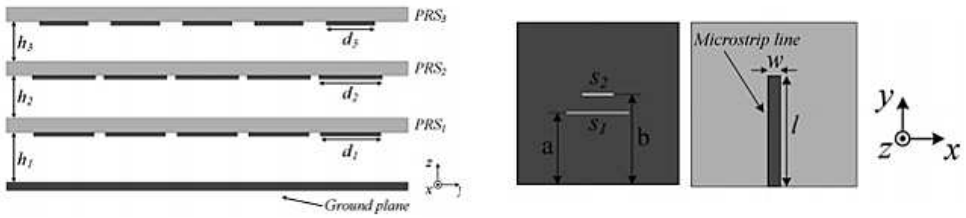

Figure 6.4: Three-Layered RCA with dual-slot feed antenna [43]

The feeding techniques proposed in [27, 43] are useful for improving the bandwidth of RCAs. However, these feeding antennas are not scalable as they tend to increase the fabrication complexities. Also, the placement of feeds in between the superstrate and ground plane affects the overall antenna performance. Practically they are not applicable to realize the sparse array configurations or to implement large arrays.

Recently, an effective method involving a dual aperture-coupled slot was proposed for feeding an RCA [44]. It employes a double-layer and three-layer superstrate forming air cavities of approximately half wavelength each in front of the ground plane as shown in Figure 6.4. The design of both superstrates is aimed to achieve a wideband impedance matching with an increased gain and directivity performance. RCAs using this method demonstrated gains of about 18.7 and 19 dBi with a 3dB gain bandwidth of 12.2% and 16% for two and three-layer antennas respectively.

Planar feeding techniques are often more desirable as compared to waveguide-fed slots in several applications such as the extension of RCAs to sparse arrays, and to reduce the overall height and cost of the antenna. This allows designing a wideband RCA with excellent directive performance as well as a well-matched feed antenna. In this research work, we evaluated the performance of single aperture-coupled slot feed and dual aperture-coupled

slot [44] feed in comparison to a waveguide-fed slot feed for use in wideband RCAs with TPG superstrates (TPGS).

6.3 Performance Evaluation of Waveguide and Planar Feeds in TPG based RCAs

Despite the ability of TPGS to provide a wide directivity bandwidth, it is essential to design a feed antenna with a wide matched bandwidth complementing the directivity bandwidth. This minimizes the mismatch loss in the RCA and provides a wide gain bandwidth, which is critical for practical applications. In order to compare the performance of each of the above-mentioned feed antennas judiciously, let us use a simple wideband RCA with a dielectric superstrate. The proposed configuration is shown in Figure 6.5. The single-layer dielectric superstrate has a radius R of $1.15\lambda_{low}$ and its thickness t is 5.3 mm. The superstrate is suspended at a height h of $0.5\lambda_{low}$ above the metallic ground plane. The wideband superstrate is radially divided into three sections of equal widths, and their dielectric constants from the innermost section to the outermost section are 9.8, 6.15 and 3.38, respectively.

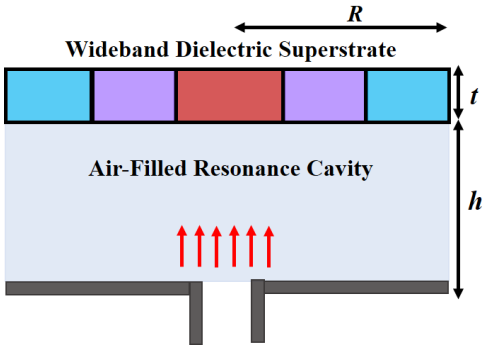

Figure 6.5: Wideband RCA with TPGS

This RCA is fed one by one using the two planar aperture-coupled slot feeding antennas and a waveguide-fed slot antenna as depicted in Figure 6.6. For waveguide feed, a single slot is made in the ground plane, and it is fed by a WR-42 waveguide to coax adaptor. Alternatively, to serve the purpose of planar feeding antennas, a low permittivity substrate (ε_r = 2.2) with the thickness of 0.787 mm was used to etch the single slot and dual slot

on the upper side of the substrate with the 50Ω transmission line at the bottom. It can be seen that the placement of single slot is exactly in the center of the ground plane whereas, both the dual slots are equidistant from the center of the ground plane with the separation of 4.47 mm. It is important to mention that the diameter of feeding antennas is same as the diameter of superstrate, and all the dimensions were fine-tuned after placing the feed antennas into the cavity. The dimensions of the waveguide-fed slot, aperture-coupled slots, and the transmission lines are calculated using the parametric analysis, as provided in Table 6.1.

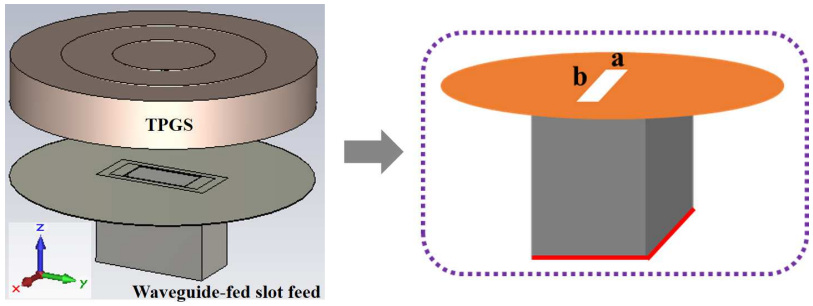

(a)

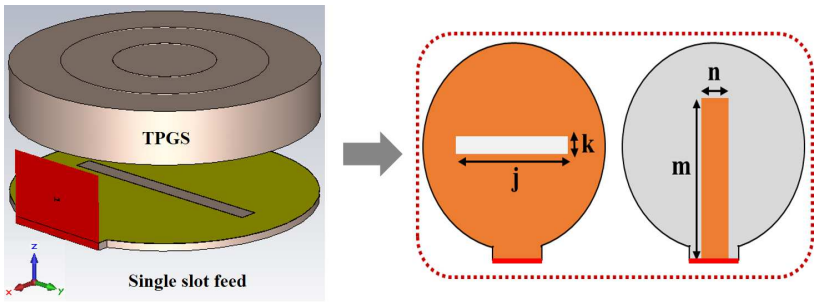

(b)

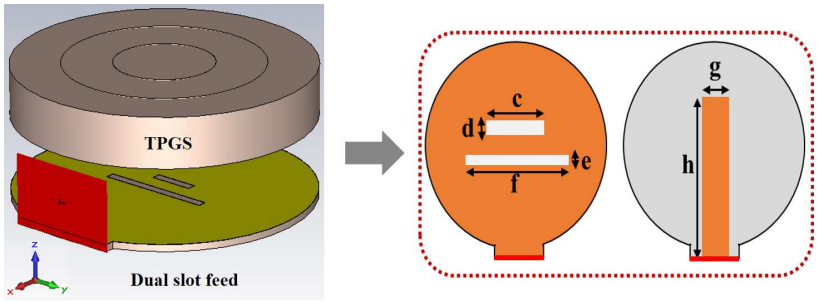

(c)

Figure 6.6: TPGS with (a) waveguide-fed slot feed (b) single slot feed (c) dual slot feed

Table 6.1: Feed antenna dimensions

Waveguide-Fed Slot Antenna	**Dual-Slot Feed Antenna**			**Single-Slot Feed Antenna**	
Slot (mm)	**Slot 1 (mm)**	**Slot 2 (mm)**	**Transmission Line (mm)**	**Slot (mm)**	**Transmission Line (mm)**
a=4	c=5	e=1	g=3	j=24	n=2.42
b=7.5	d=1	f=13	h=20.41	k=2	m=18.41

6.4 Numerical Results and Discussion

6.4.1 Impedance Bandwidth

Full-wave simulations for each case discussed above were conducted in CST Microwave Studio. To illustrate the narrow-band behavior of the feeding antenna, the input reflection coefficient ($|S_{11}|$) of a circular patch antenna is shown in Figure 6.7. It can be seen that the circular patch provides a very narrow bandwidth from 22.24 - 22.83 GHz. The $|S_{11}|$ of both single and dual aperture-coupled slot feed antenna is also shown in Figure 6.7, predicting a much wider matched bandwidth. It can be obsserved that the matched bandwidth extends from 20.94 - 24.03 GHz and 20.47 - 24.19 GHz for each aperture-coupled slotted feed antenna. It is important to mention that the $|S_{11}|$ in Figure 6.7 of the feeding antennas are computed in free space, i.e., without the superstrate loading. After achieving the desired broadband response, the corresponding single slot and dual slot feed antennas were placed in the cavity of the TPG based RCA. The dimensions of slots were then fine-tuned again to increase the matched bandwidth, and the performance was compared with the waveguide-fed slot feed. The $|S_{11}|$ of all the three feeds under investigation is presented in Figure 6.8. TPGS with waveguide-fed slot depicts broadband bandwidth extending from 20.67 - 25.00 GHz in comparison to the TPGS with single aperture-coupled slot feed, which achieves the bandwidth response of 20.81 - 25.32 GHz. It is interesting to note that the TPGS with dual aperture-coupled slot attains the highest matched bandwidth ranging from 20.81 - 25.32 GHz.

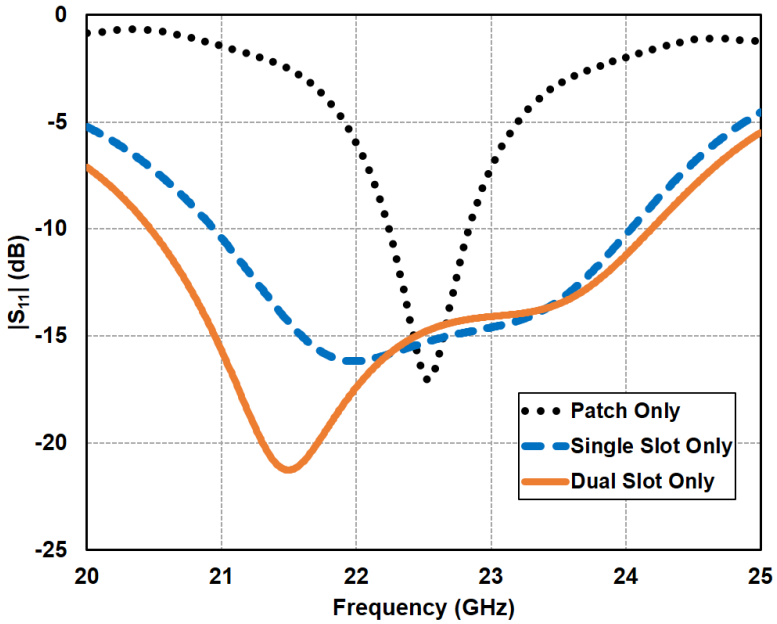

Figure 6.7: Input reflection coefficient of the feed antennas in free space (without superstrate)

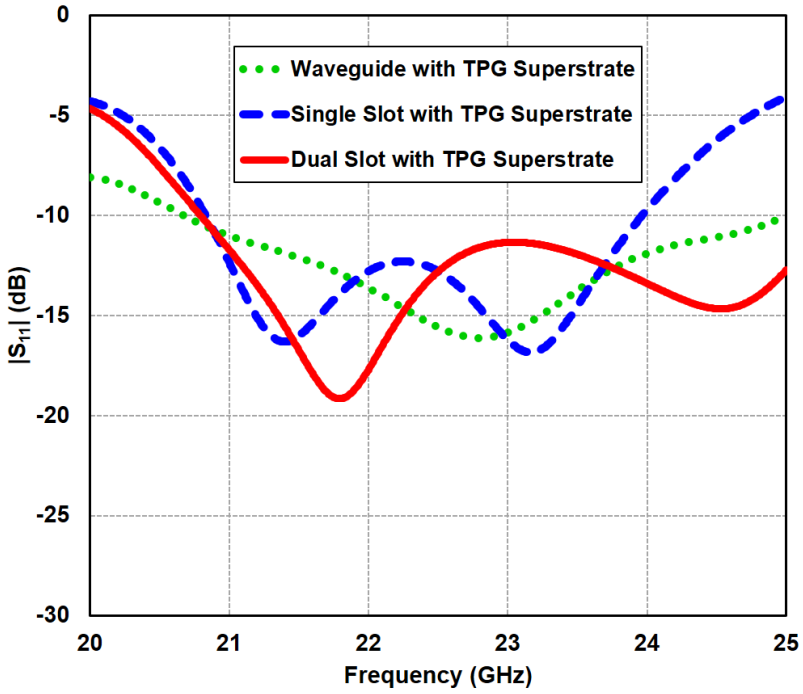

Figure 6.8: Input reflection coefficient of the feed antennas with superstrate loading (small plot in red shows the complete range for $|S_{11}|$ below -10dB)

Table 6.2: Comparison of impedance bandwidth of feed antennas with and without TPGS

Feed Antenna	Bandwidth Range (GHz)	% Bandwidth
Waveguide with TPG Superstrate	20.67 - 25.00	19.3
Single Slot with TPG Superstrate	20.83 - 23.96	13.9
Dual Slot with TPG Superstrate	20.81 - 25.32	20.1

The impedance bandwidth of the demonstrated feeding antennas is summarized in Table 6.2. The loading effect of the superstrate on the feed antennas provided the widest matched bandwidth of 20.1% with dual slot feed. We have also found that waveguide feed contributed the second highest impedance bandwidth of 19.3% followed by single slot feed achieving 13.9% bandwidth. The percentage bandwidth values of the feeding antennas may vary considering the fact that they should cover the whole operating band without significantly affecting the directivity bandwidths of the RCAs, as compared in the next section.

6.4.2 Directivity Bandwidth

The computed directivities for each of the feeding configurations are compared in Figure 6.9. It can be seen from Figure 6.9 that the waveguide-fed slot predicts a peak directivity of 18.6 dBi with 3dB directivity-bandwidth of more than 20%. Whereas, in case of the single and dual aperture-coupled slot, the directivity reaches a maximum of 16.2 dBi and 17 dBi along with a 3dB directivity bandwidth of 16.2% and 15% respectively. The results predict an approximate difference of 1.6 dBi and 0.6 dBi in the maximum directivity for the waveguide feed and aperture-coupled slotted feeds. The difference is caused by the fact that the waveguide induces minimal losses as it is filled with air, whereas the printed feed is more prone to increased losses within the dielectric material. In addition, considering the small size of the ground plane, the printed transmission line may give rise to spurious radiations which reduce the coupling of electromagnetic energy to the cavity, thereby reducing boresight directivity of the RCA. Thus, the decrease in the directivity is due to the inherent resonance of the slots and the backward radiations which was not in the case of waveguide feeds. It is envisaged that this undesired radiation can be reduced by using a stripline feed instead of a

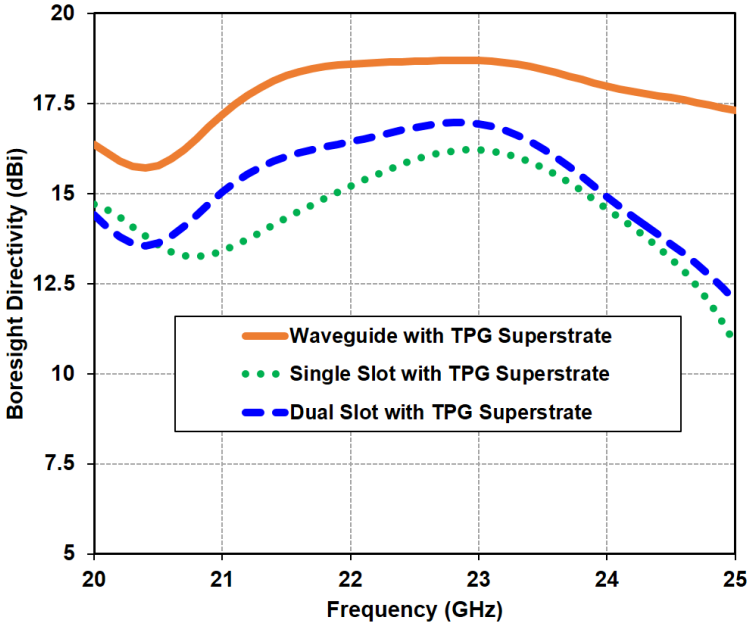

Figure 6.9: Comparison of boresight directivity for RCA with different feeding antennas

microstrip transmission line.

6.4.3 Far-field Radiation Patterns

The radiation patterns of the RCA with feeding antennas at the center frequency of 22.4 GHz are depicted in Figure 6.10 for the two principal planes. It is evident that each feed antenna attains well-directed boresight beam with appropriate side lobe levels (SLLs). The SLLs in E-plane remains around -17 dB for waveguide feed, -16 dB for single slot feed and -13 dB for dual slot feed. On the other hand, the SLLs in H-Plane reaches to -20 dB, -14 dB and -15 dB respectively. However, comparing the radiation patterns of both planar feeds, one may notice a slight variation in the beam pattern of dual slot feed as it appears to be slightly skewed towards left. This variation can be attributed to the structural tolerances such as the varying slot dimensions on the ground plane. The dual slot feed has two different length slots offset from the centre, which works to increase the bandwidth because of the offset resonances of the two length slots. This inherently adds asymmetry to the feed.

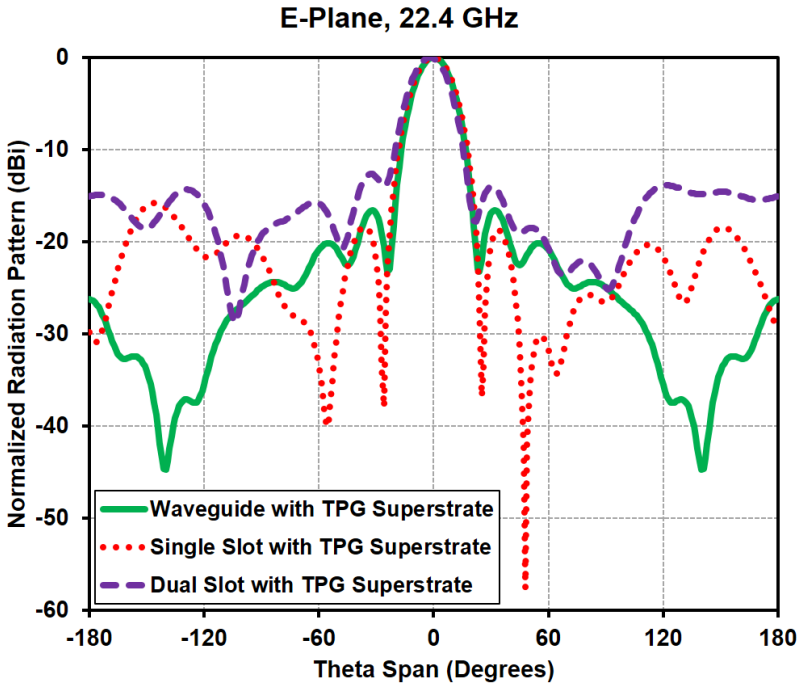

(a)

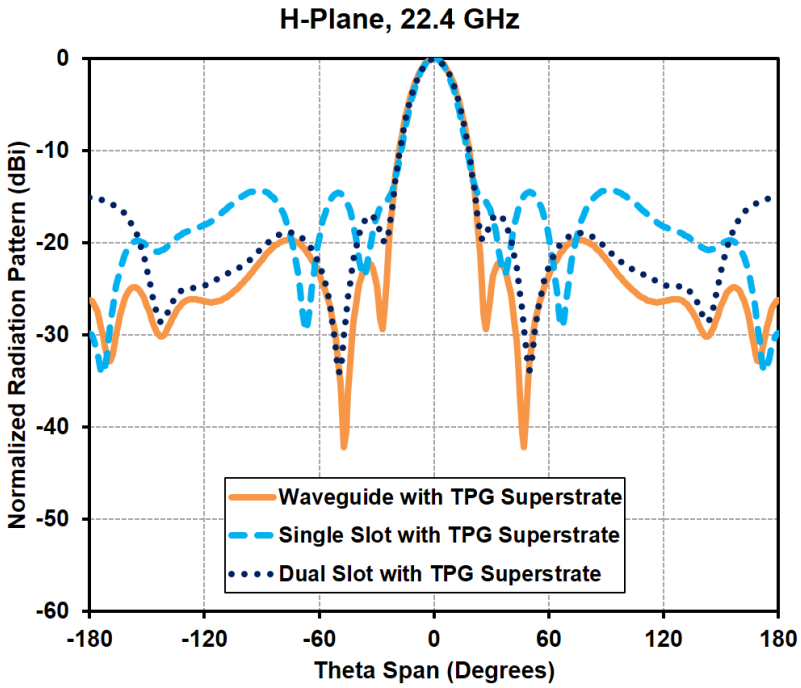

(b)

Figure 6.10: Normalized radiation patterns of the RCA with waveguide and planar feeds (a) E-Plane at 22.4 GHz (b) H-Plane at 22.4 GHz

6.5 Conclusion

An effective planar feeding method based on single/dual aperture-coupled slot feed antennas is compared with conventional waveguide-fed slot feed when used in wideband RCAs. Planar feed antennas achieve approximately $0.6\lambda_{low}$ RCA height reduction as compared to waveguide-fed slot. They also exhibited a peak directivity of 16.2 dBi and 17 dBi along with a 3dB directivity bandwidth of 16.2% and 15% respectively. The planar feeding technique addressed few limitations associated with the waveguide-fed slot by reducing the overall antenna profile and is cost effective. Moreover, it is well suited for the sparse arrays or switched-polarization array configurations.

Chapter 7

Conclusions and Future Work

7.1 Conclusions

RCA is a class of highly-directive antennas well known for its simple configuration. RCAs are being viewed as the emerging candidates for use in fixed communication systems including back-haul networks, point-to-point microwave links and satellite reception. However for the commercial deployment, these antennas are required to meet the stringent requirements to conform to the suitable gain and radiation pattern envelope (RPE) specifications, as documented by the regulatory bodies.

This thesis presented research on the design of wideband and high-gain resonant cavity antenna arrays (RCAAs) and highlighted their potential to approach the minimum ETSI class-2[1] antenna requirements. Initially, a single RCA element was designed. It was fed using a waveguide and has superstrate areas as small as $2.3\lambda_{low}$. This RCA features a single-layer dielectric superstrate with radially non-uniform permittivity in the transverse plane. A computed 3dB directivity bandwidth of 49.31% was obtained with the peak directivity of 18.7 dBi. Analytical predictions demonstrated the suitability of designing an array with the proposed RCA element by placing them in close proximity. Following this approach, full-wave simulations were carried out to verify the array factor estimations. In comparison to a 9×9 square array, Tier7 radial array (having 91 elements) is shown to achieve the peak directivity of 37dBi with a directivity bandwidth of more than 20%. Furthermore,

[1]Standard back-haul antennas for fixed wireless communications

far-field patterns have showcased the potential of RCAAs to satisfy the minimum ETSI Class-2 antenna requirements with appropriate RPEs and SLLs as low as -17 dBi. The simple and planar configuration of such arrays makes them highly suitable for various fixed wireless communication applications, considering their small footprint area and low-profile characteristics.

Following this, another technique was investigated to design a phase correcting surface (PCS) for the performance enhancement of RCAAs. A case study was conducted to implement the PCS on a 3×3 square array depicting an improvement in the directivity and SLLs at a center frequency of 22.3 GHz. In addition, planar feeding configurations including single and dual aperture coupled slots were also investigated to replace the conventional waveguide feeds. RCAs with waveguide feeds are very expensive when used to design arrays. Therefore, planar feeding methods while achieving comparable performance are invaluable to the design of RCAAs. The design of such feed antennas reduces the overall height, making them light-weight and low-cost, and ease the fabrication of sparse arrays or switched-polarization arrays with printed feed networks.

7.2 Future Work

The following aspects of RCAs and RCAAs can be considered for further research and development:

- Planar feeding configurations can be extended to design a corporate feed network for RCAAs.
- The polarization versatility of dielectric-only RCAs can be exploited to support circular polarization (CP). For this purpose, CP feeds can be designed to achieve wide axial-ratio (AR) within the targeted directivity bandwidth.
- The proposed RCAA can be investigated with various beam-steering techniques in order to meet the growing demands of next-generation wireless systems.

Appendix A

List of Acronyms

AMC	Artificial Magnetic Conductor
CST	Computer Simulation Technology
CST MWS	CST Microwave Studio
EBG	Electromagnetic Band Gap
ERA	EBG Resonator Antenna
ETSI	European Telecommunications Standards Institute
FSS	Frequency Selective Surface
PRS	Partially Reflecting Surface
RCA	Resonant Cavity Antenna
RCAA	Resonant Cavity Antenna Array
RPE	Radiation Pattern Envelope
SLL	Side Lobe Level
TPG	Transverse Permittivity Gradient
TPGS	Transverse Permittivity Gradient Superstrate

References

[1] M. Thevenot, C. Cheype, A. Reineix, and B. Jecko, "Directive photonic-bandgap antennas," *IEEE Transactions on Microwave Theory and Techniques*, vol. 47, no. 11, pp. 2115–2122, 1999.

[2] Y. Ge and K. P. Esselle, "A resonant cavity antenna based on an optimized thin superstrate," *Microwave and Optical Technology Letters*, vol. 50, no. 12, pp. 3057–3059, 2008.

[3] A. R. Weily, K. P. Esselle, B. C. Sanders, and T. S. Bird, "High-gain 1D EBG resonator antenna," *Microwave and Optical Technology Letters*, vol. 47, no. 2, pp. 107–114, 2005.

[4] M. Qiu and S. He, "High-directivity patch antenna with both photonic bandgap substrate and photonic bandgap cover," *Microwave and Optical Technology Letters*, vol. 30, no. 1, pp. 41–44, 2001.

[5] C. Serier, C. Cheype, R. Chantalat, M. Thevenot, T. Monediere, A. Reineix, and B. Jecko, "1-D photonic bandgap resonator antenna," *Microwave and optical technology letters*, vol. 29, no. 5, pp. 312–315, 2001.

[6] H. Yang and N. Alexopoulos, "Gain enhancement methods for printed circuit antennas through multiple superstrates," *IEEE Transaction on Antennas and Propagation*, vol. 35, no. 7, pp. 860–863, 1987.

[7] G. Trentini, "Partially reflecting sheet arrays," *IEEE Transaction on Antennas and Propagation*, vol. 4, no. 4, pp. 666–671, 1956.

[8] A. P. Feresidis and J. C. Vardaxoglou, "High gain planar antenna using optimised

partially reflecting surfaces," *IEEE Proceedings on Microwaves, Antennas and Propagation*, vol. 148, no. 6, pp. 345–350, 2001.

[9] M. Rahman and M. Stuchly, "Transmission line-periodic circuit representation of planar microwave photonic bandgap structures," *Microwaves and Optical Technology Letter*, vol. 30, no. 1, pp. 15–19, 2001.

[10] R. Gardelli, M. Albani, and F. Capolino, "Array thinning by using antennas in a Fabry-Perot cavity for gain enhancement," *IEEE Transactions on Antennas and Propagation*, vol. 54, no. 7, pp. 1979–1990, 2006.

[11] C. Cheype, C. Serier, M. Thevenot, T. Monediere, A. Reineix, and B. Jecko, "An electromagnetic bandgap resonator antenna," *IEEE Transaction on Antennas and Propagation*, vol. 50, no. 9, pp. 1285–1290, 2002.

[12] Z. G. Liu, Z. C. Ge, and X. Y. Chen, "Research progeress on Fabory-Perot resonator printed antenna," *Science A*, vol. 10, no. 4, pp. 12–17, 2006.

[13] D. Jackson and A. Oliner, "A leaky-wave analysis of the high-gain printed antenna configuration," *IEEE Transaction on Antennas and Propagation*, vol. 36, no. 7, pp. 905–910, July 1998.

[14] D. R. Jackson, P. Burghignoli, G. Novat, F. Capolino, C. Ji, D. R. Wilton, and A. A. Oliner, "The fundamental physics of directive beaming at microwave and optical frequencies and the role of leaky waves," *IEEE Proceedings*, vol. 99, no. 10, pp. 1780–1805, 2011.

[15] B. A. Zeb, R. M. Hashmi, K. P. Esselle, and Y. Ge, "The use of reflection and transmission models to design wideband and dual-band Fabory-Perot cavity antennas," *URSI International Symposium on Electromagnetic Theory*, pp. 1084–1087, 2013.

[16] R. M. Hashmi, B. A. Zeb, and K. P. Esselle, "Composite defect-mode superstructures and wideband EBG resonator antennas," *9th European Conference on Antennas and Propagation (EuCAP)*, pp. 1–5, 2015.

[17] A. Weily, K. Esselle, T. Bird, and B. Sanders, "Dual resonator 1-D EBG antenna with slot array feed for improved radiation bandwidth," *IET Microwaves, Antennas & Propagation*, vol. 1, no. 1, pp. 198–203, 2007.

[18] N. Guérin, S. Enoch, G. Tayeb, P. Sabouroux, P. Vincent, and H. Legay, "A metallic Fabry-Perot directive antenna," *IEEE Transactions on Antennas and Propagation*, vol. 54, no. 1, pp. 220–224, 2006.

[19] L. Moustafa and B. Jecko, "Broadband high gain compact resonator antennas using combined FSS," *IEEE International Symposium on Antennas and Propagation Society (APS)*, pp. 1–4, 2008.

[20] Z. Liu, W. Zhang, D. Fu, Y. Gu, and Z. Ge, "Broadband Fabry-Perot resonator printed antennas using FSS superstrate with dissimilar size," *Microwave and Optical Technology Letters*, vol. 50, no. 6, pp. 1623–1627, 2008.

[21] S.-C. Chiu and S.-Y. Chen, "High-gain circularly polarized resonant cavity antenna using FSS superstrate," *IEEE International Symposium on Antennas and Propagation (APS/URSI)*, pp. 2242–2245, 2011.

[22] A. R. Weily, L. Horvath, K. P. Esselle, B. C. Sanders, and T. S. Bird, "A planar resonator antenna based on a woodpile EBG material," *IEEE Transactions on Antennas and Propagation*, vol. 53, no. 1, pp. 216–223, 2005.

[23] Y. J. Lee, J. Yeo, R. Mittra, and W. S. Park, "Application of electromagnetic bandgap (EBG) superstrates with controllable defects for a class of patch antennas as spatial angular filters," *IEEE Transactions on Antennas and Propagation*, vol. 53, no. 1, pp. 224–235, 2005.

[24] L. Leger, T. Monediere, and B. Jecko, "Enhancement of gain and radiation bandwidth for a planar 1-D EBG antenna," *IEEE Microwave and Wireless Components Letters*, vol. 15, no. 9, pp. 573–575, 2005.

[25] A. Feresidis and J. Vardaxoglou, "A broadband high-gain resonant cavity antenna with single feed," *First European Conference on Antennas and Propagation (EUCAP)*, 2006.

[26] M. A. Al-Tarifi, D. E. Anagnostou, A. K. Amert, and K. W. Whites, "Bandwidth enhancement of the cavity resonance antenna (CRA) using multiple dielectric superstrate layers," *IEEE MTT-S International Symposium Digest on Microwave (MTT)*, pp. 1–4, 2011.

[27] Y. Ge, K. P. Esselle, and T. S. Bird, "The use of simple thin partially reflective surfaces with positive reflection phase gradients to design wideband, low-profile EBG resonator antennas," *IEEE Transactions on Antennas and Propagation*, vol. 60, no. 2, pp. 743–750, February 2012.

[28] R. M. Hashmi, B. A. Zeb, and K. P. Esselle, "Wideband high-gain EBG resonator antennas with small footprints and all-dielectric superstructures," *IEEE Transactions on Antennas and Propagation*, vol. 62, no. 6, pp. 2970–2977, June 2015.

[29] R. M. Hashmi and K. P. Esselle, "A class of extremely wideband resonant cavity antennas with large directivity-bandwidth products," *IEEE Transaction on Antennas and Propagation*, vol. 64, no. 2, pp. 830–835, February 2016.

[30] S. A. Muhammad, R. Sauleau, and H. Legay, "Small-size shielded metallic stacked Fabry–Perot cavity antennas with large bandwidth for space applications," *IEEE Transactions on Antennas and Propagation*, vol. 60, no. 2, pp. 792–802, 2012.

[31] R. M. Hashmi and K. P. Esselle, "A wideband EBG resonator antenna with an extremely small footprint area," *Microwave and Optical Technology Letters*, vol. 57, no. 7, pp. 1531–1535, 2015.

[32] R. Hashmi and K. Esselle, "Arrays of high aperture efficiency wideband EBG resonator antennas," *IEEE International Conference on Electromagnetics in Advanced Applications (ICEAA)*, pp. 942–944, 2015.

[33] M. U. Afzal, K. P. Esselle, and A. Biswas, "A method to enhance radiation characteristics by improving aperture phase distribution of electromagnetic bandgap resonator antennas," *IEEE International Conference on Electromagnetics in Advanced Applications (ICEAA)*, pp. 561–564, 2015.

[34] H. D. Hristov and H. Herben, "Millimeter-wave fresnel-zone plate lens and antenna," *IEEE Transactions on Microwave Theory and Techniques*, vol. 43, no. 12, pp. 2779–2785, 1995.

[35] Y. Ji and M. Fujita, "Design and analysis of a folded fresnel zone plate antenna," *International Journal of Infrared and Millimeter Waves*, vol. 15, no. 8, pp. 1385–1406, 1994.

[36] Y. Zhang, R. Mittra, and W. Hong, "Systematic design of planar lenses using artificial dielectrics," in *IEEE International Symposium on Antennas and Propagation Society*, 2010.

[37] S. Jain, M. Abdel-Mageed, and R. Mittra, "Flat-lens design using field transformation and its comparison with those based on transformation optics and ray optics," *Antennas and Wireless Propagation Letters, IEEE*, vol. 12, pp. 777–780, 2013.

[38] M. U. Afzal, K. P. Esselle, and B. A. Zeb, "Dielectric phase-correcting structures for electromagnetic band gap resonator antennas," *IEEE Transactions on Antennas and Propagation*, vol. 63, no. 8, pp. 3390–3399, 2015.

[39] M. U. Afzal and K. P. Esselle, "Improving phase uniformity in the aperture: A method to enhance radiation characteristics of Fabry-Perot resonator antennas," *IEEE International Symposium on Antennas and Propagation & USNC/URSI National Radio Science Meeting*, pp. 39–40, 2015.

[40] B. A. Zeb, R. M. Hashmi, and K. P. Esselle, "Wideband gain enhancement of slot antenna using one unprinted dielectric superstrate," *IEEE Electronics Letter*, vol. 51, no. 15, pp. 1146–1148, July 2015.

[41] A. A. Baba, R. M. Hashmi, and K. P. Esselle, "Wideband gain enhancement of slot antenna using superstructure with optimised axial permittivity variation," *IEEE Electronics Letter*, vol. 52, no. 4, pp. 266–268, February 2016.

[42] C. A. Balanis, *Antenna Theory: Analysis and Design*, 4th ed. Wiley, 2015.

[43] N. Wang, J. Li, G. Wei, L. Talbi, Q. Zeng, and J. Xu, "Wideband Fabry-Perot resonator antenna with two layers of dielectric superstrates," *IEEE Antennas and Wireless Propagation Letters*, vol. 14, pp. 229–232, 2015.

[44] K. Konstantinidis, A. P. Feresidis, and P. S. Hall, "Dual-slot feeding technique for broadband Fabry-Perot cavity antennas," *IET Microwaves, Antennas & Propagation*, vol. 9, no. 9, pp. 861–866, 2015.